The Role of PARylation in Inflammatory Mediated Subclass of Preeclampsia

Sophia Vanegas Pineda

A thesis submitted to the University of Ottawa in partial fulfilment of the requirements for the degree Master of Science of Biochemistry

uOttawa

School of Biochemistry, Microbiology, and Immunology

Faculty of Medicine

University of Ottawa

ABSTRACT

Preeclampsia (PE) is a leading cause of maternal and neonatal morbidity and mortality, diagnosed after 20 weeks of gestation. Several subclasses of PE have been identified, each with distinct pathophysiology. Notably, the inflammation-mediated subclass (I-PE) is characterized by a pronounced increase in placental PARylation and a marked depletion of NAD^+. This study investigates the mechanistic basis of this phenotype by profiling placental NAD^+-consuming enzymes and assessing whether selective inhibition of PARylating enzymes can restore trophoblast function and placenta health. HTR-8/SVneo trophoblast cells were exposed to TNF-α to mimic the I-PE inflammatory environment in vitro. Cells were also co-treated with Olaparib (a PARP1/2 inhibitor) or XAV939 (a PARP5a/5b inhibitor), as PARP1/2 and PARP5a/5b have been identified as key PARylating enzymes in the placenta. Total protein PARylation, cellular viability, mitochondrial function, and migratory capacity were assessed as cellular health and functional outcomes. TNF-α exposure increased total protein PARylation and impaired mitochondrial health by decreasing oxygen consumption rates during respiration, cellular viability and migration. Co-treatment with Olaparib reduced protein PARylation within 1h and restored cellular viability and migration, and mitochondrial respiration despite the continued pro-inflammatory conditions. In contrast, co-treatment with XAV939 showed no improvement in cellular health or function. These findings suggest that inflammation-induced PARP1/2 activation may contribute to placental PARylation and NAD^+ depletion in I-PE and highlight the PARP1/2- NAD^+ axis as a potential therapeutic target to improve placental health and function in affected pregnancies.

ACKNOWLEDGMENTS

Science is beautiful in all its complexity and forms. It is a privilege we have to learn, ask, find answers and contribute to the current building blocks that have allowed us to understand the world, shaping our understanding of life. Every researcher knows that science has a way of sitting us down and humbling us with its complexity by reminding us of how much we have yet to understand. Despite all of our doubts, failures, and challenges we faced – there are moments of reward where we thank our curiosity for leading us here. It is with that same curiosity that led me to study one of the foundations of life, the placenta. The privilege I've had to study and understand the placenta in all its beauty and form is truly humbling and deepened my respect for mothers. Without placenta there would be nothing! After writing my thesis, the acknowledgement is the section I was most excited to write about because of all the wonderful people who supported me through this journey that I want to thank.

First and foremost, I would like to express my deepest gratitude's to my amazing supervisors, Dr. Shannon Bainbridge and Dr. Keir Menzies for their endless encouragement, guidance and patience throughout this thesis project. You have not only shaped this project but also guided my development as a researcher that will leave an impact beyond the lab. Both of you have given me the privilege to travel and attend conferences that have strengthen my curiosity and inspired me to become a better scientist. Thank you for all the lab outings you both have organized and for creating a great safe space for young investigators, including myself. Secondly, I am grateful for my TAC committee, Dr. David Landry and Dr. Alexander Blais for your tremendous help and guidance on this thesis. Thank you for attending each TAC meeting, providing me with thoughtful feedback on my presentations and my progress reports. Your insights and perspectives have greatly strengthened the quality and clarity of this project.

I would like to thank the members of the Placenta Lab and the Menzies lab, including all the undergrads and grad students who have offered their great advice, support and motivation. A huge thanks to Yusmaris Cariaco and Abolfazl Nik-Akhtar for helping me troubleshoot countless problems, generously sharing your knowledge, keeping everyone in the lab motivated and giving your previous time and energy. It has been a pleasure working alongside the both of you – you both are the truly the glue that holds the lab together. Big thanks to Ghofrane El Moatassim and Lanna Kadhim – those late nights at the lab are memories I'll always cherish. Thank you to Jade Gamelin Kao, Hannah Poisson, Anastasia Pisanko and Kejzi Saraci for all the nights out that have always ended at the karaoke bar each time.

To my Goulburn family and friends – you know who you are – a huge thanks to every single one of you for always listening to my endless rants from cell culture to PCR experiments and for keeping me motivated throughout this crazy journey. Thank you for making Ottawa fun and full of memories I'll never forget.

Most importantly, I would like to thank my mother, father and sister for all their endless love, support and patience. Even though we were 400 km apart, I always felt your presence and encouragement. None of this would be possible without all of you. Thank you for always answering my calls and listening to me troubleshoot my western blots issues for 3 hours. Thank you for always believing in me.

LIST OF FIGURES

LIST OF TABLES

LIST OF ABBREVIATIONS

4HNE	4-hydroxynonenal
8-OXO-dG	8-Oxo-2'-deoxyguanosine
ADP	Adenosine diphosphate
AGA	Appropriate for Gestational Age
AMPK	AMP-activated protein kinase
AMP	Adenosine monophosphate
ATP	Adenosine triphosphate
BRCA	Breast Cancer gene
BSA	Bovine serum albumin
CD68	Cluster of Differentiation 68
CD8	Cluster of Differentiation 8
CKD	Chronic Kidney disease
CTB	Cytotrophoblast
DMSO	Dimethyl sulfoxide
DNA	Deoxyribonucleic acid
DSB	Double-strand break
ERK	Extracellular signal-regulated Kinase
ETC	Electron transport chain
EVT	Extravillous trophoblast
FBS	Fetal bovine serum
FCCP	Carbonyl cyanide p-trifluoro-methoxyphenyl hydrazone
FGR	Fetal growth restriction
FLT-1	Vascular endothelial growth factor receptor 1
GD	Gestation Day
H-PE	Hypoxia-mediated preeclampsia
H2O2	Hydrogen Peroxide
I-PE	Inflammation-mediated preeclampsia
IL-10	Interleukin-10
IL-14	Interleukin-14
IL-17	Interleukin-17
IL-6	Interleukin-6
LC-MS	Liquid Chromatography Mass Spectrometry
LPS	Lipopolysaccharides
M-PE	Maternal-mediated preeclampsia
MAPK	Mitogen-activated protein kinase
MAR	Mono-ADP-ribose
MPO	Myeloperoxidases
MS	Mass spectrometry
MTCO1	Mitochondrially encoded cytochrome c oxidase I
mtDNA	Mitochondrial DNA
NA	Nicotinic acid
NAD^+	Nicotinamide adenine dinucleotide

NADt	NAD total
NAM	Nicotinamide
NF-κB	Nuclear factor-kappa B
NR	Nicotinamide riboside
OCR	Oxygen consumption rate
OXPHOS	Oxidative phosphorylation
P/S	Penicillin/Streptomycin
PAR	Poly ADP-ribose
PARP-1	Poly (ADP-ribose) polymerase-1
PARP-2	Poly (ADP-ribose) polymerase-2
PARP-7	Poly (ADP-ribose) polymerase-7
PARP-10	Poly (ADP-ribose) polymerase-10
PARP-12	Poly (ADP-ribose) polymerase-12
PARP-14	Poly (ADP-ribose) polymerase-14
PARPi	Poly (ADP-ribose) polymerase-inhibitor
PBS	Phosphate-buffered saline
PCR	Polymerase chain reaction
PE	Preeclampsia
PGC-1α	Peroxisome proliferator-activated receptor gamma coactivator 1-alpha
PUFA	Polyunsaturated fatty acid
RCWIH	Research Centre for Women's and Infants' Health
RIN	RNA integrity number
RIPA	Radioimmunoprecipitation assay
RNA	Ribonucleic acid
ROS	Reactive species oxygen
RT-qPCR	Reverse-transcription Quantitative polymerase chain reaction
SDHB	Succinate dehydrogenase subunit B
SDS-PAGE	Sodium dodecyl sulfate-polyacrylamide gel electrophoresis
SIRT-1	Sirtuin-1
SIRT-2	Sirtuin-2
SIRT-3	Sirtuin-3
SIRT-4	Sirtuin-4
SIRT-5	Sirtuin-5
SSB	Single-stranded stranded binding
TBS-T	Tris-buffered saline-Tween20
TCA	Tricarboxylic acid cycle
TNF-A	Tumor necrosis factor
TNFR	Tumor necrosis factor receptor
TNKS-1	Tankyrase-1
TNKS-2	Tankyrase-1
TSA	Trichostatin A
VEGF	Vascular Endothelial growth factor
WNT	Wingless-related integration site

TABLE OF CONTENTS

1 Introduction

1.1 Preeclampsia: Clinical Significance and Epidemiology

Preeclampsia (PE) is a complex hypertensive disorder of pregnancy and is a leading cause of maternal and fetal mortality and morbidity worldwide.[1] It complicates approximately 5-10% of pregnancies globally, with a higher prevalence reported in low to middle-income countries.[1] Each year, over 40,000 maternal deaths and more than 500,000 combined fetal and neonatal deaths are attributed to PE.[1] In Canada, the prevalence of hypertensive disorder in pregnancy increased from 6.1% to 8.5% between 2012 and 2021, reflecting a rising public health concern even in higher-income settings.[2] PE is diagnosed after 20 weeks of gestation and is defined by new-onset hypertension (systolic blood pressure ≥ 140 or diastolic blood pressure ≥ 90 mmHg . In addition to elevated blood pressure, PE presents with signs of maternal-end organ dysfunction, including proteinuria, thrombocytopenia, elevated liver enzymes, and other systemic abnormalities.[2,3,4] These features emphasize the multisystemic and complexity of this disorder as well as its variability in presentation and severity. Currently, the only treatment for PE is delivery, regardless of gestational age.[2,5,6] While delivery can be lifesaving, preterm birth and the often-associated fetal growth restriction (FGR) can increase the risk of long-term complications, neurodevelopmental delays, cardiovascular dysfunction, and altered immune system development in the child. [2,6,7] Moreover, PE can have long-lasting consequences for the mother, including an increased risk of major cardiovascular events[6,8], chronic kidney disease (KD)[2] , liver failure[4], and metabolic or endocrine disorders in the postpartum period[3].

1.2 Pathophysiology and Subtypes of Preeclampsia

Historically, the etiology of PE was thought to originate from an abnormal placental perfusion, resulting from the incompletion of spiral artery remodelling.[9,10] Normally, the fetal-placental circulation system is established within the first 12 weeks of gestation, when maternal blood starts to flow into the intervillous space surrounding the fetal chorionic villi, encasing the fetal capillary networks **(Figure 1)**.[10–12] This process is essential to meet the required gas and nutrient exchange between the mother and fetus.[10,13–15] The establishment of this circulation depends on differentiation of placental cytotrophoblast cells into specialized extravillous trophoblast cells (EVTs).[14,16,17] EVTs migrate and invade the maternal decidua to initiate vascular remodelling of the uterine spiral arteries that is crucial for the development of healthy placental **(Figure 1)**. [6,14,16,17] During this process, EVTs replace endothelial and smooth muscle cells that are lining the arteries, and transform them into high-capacity, low-resistance vessels that are no longer responsive to any circulating vasopressors.[6,14,16,18–20] This remodelling facilitates the maternal blood flow into the placenta to meet the growing demands of the fetus.

In the traditional model of PE pathogenesis, when this remodelling process is incomplete or defective, the placental blood flow is reduced and leads to placental hypoxia and oxidative stress **(Figure 1)**.[3,5–9] In response, the dysfunctional placenta releases a wide range of pro-inflammatory cytokines[21–23], anti-angiogenic factors[23–26] (such as FLT-1 and endoglin), oxidative stress mediators[23,27,28], and placental cell debris, including material from apoptotic and necrotic trophoblasts cells. These factors enter the maternal circulation, triggering systemic endothelial dysfunction, heightened inflammation, and the characteristic clinical features of PE-hypertension, proteinuria, and end-organ injury.[29,30] This has given rise to the “two-stage model” of PE:

- Stage 1 occurs in the first trimester and involves poor placentation and abnormal spiral artery remodeling.[6]
- Stage 2 arises later in pregnancy, in the second or third trimester, when maternal systemic responses to placental signals lead to disease.[6]

However, emerging evidence suggests that this model may not fully capture the heterogeneity of PE. Approximately 40% of PE cases do not show any evidence of impaired spiral artery remodelling, challenging the historical paradigm.[31,32] Moreover, no single circulating biomarker has proven effective for early prediction or diagnosis of PE, and no clinical trial aimed at preventing or treating PE has consistently demonstrated success, particularly across diverse patient populations.

These findings have led researchers to re-evaluate the classical paradigm, proposing instead that PE represents a syndrome with multiple subtypes, each with distinct molecular origins and clinical trajectories. Some forms of PE may be primarily placenta-driven, while others could be rooted in maternal cardiovascular, metabolic, or immune dysfunction, or inflammatory pathways that precede or occur independently of placental abnormalities. This evolving perspective underscores the need to define and study molecularly distinct subclasses of PE, which may ultimately pave the way for personalized diagnostics, risk stratification, and targeted interventions.

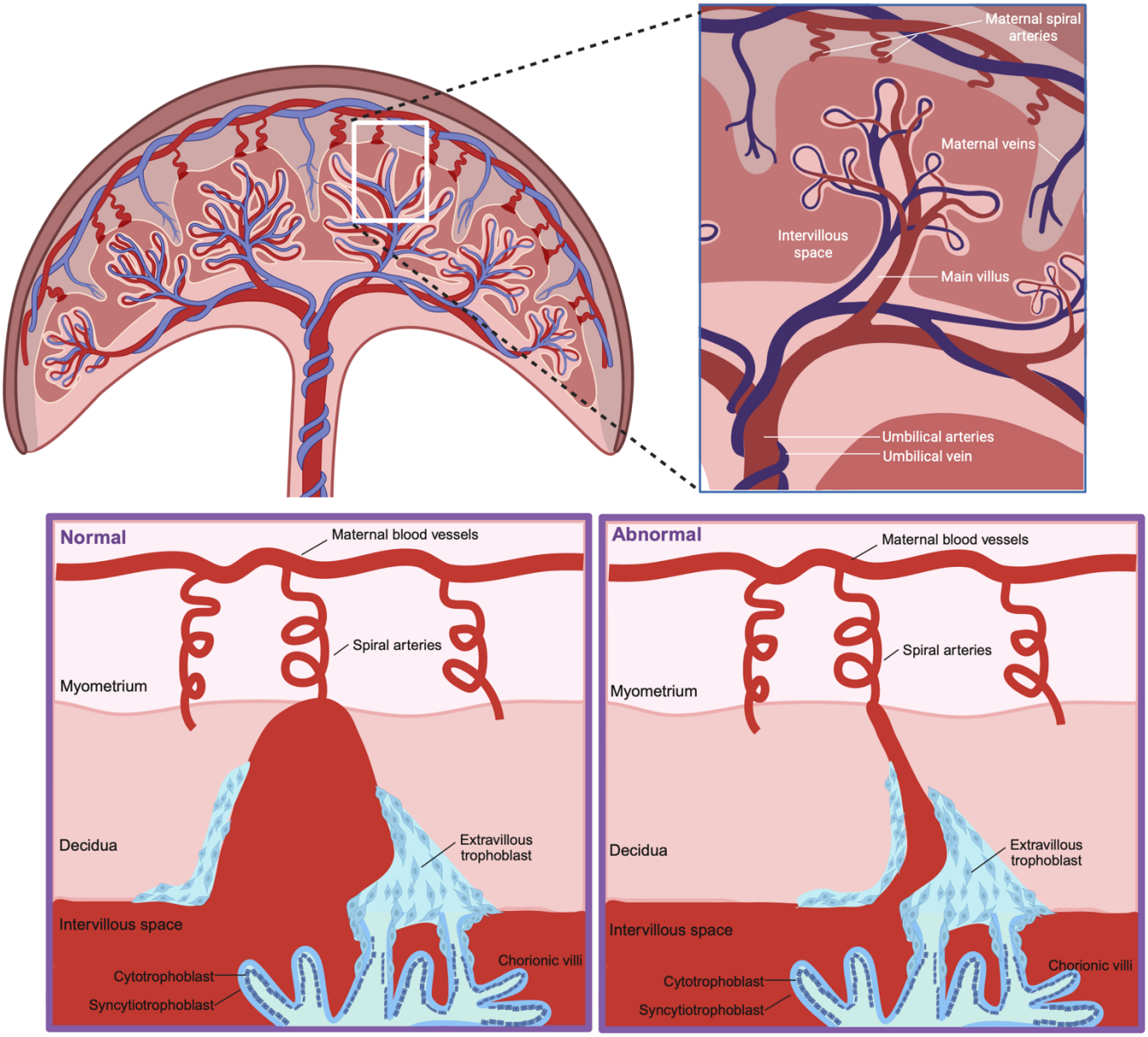

Figure 1. Schematic of Utero-Placental Circulation. (A) Schematic of placenta (left) and the maternal-fetal circulation (right), where maternal oxygenated blood is delivered into intervillous space surrounding the chorionic villi. **(B)** In normal pregnancy, spiral artery undergoes artery remodelling to allow sufficient blood to the intervillous space. Extravillous trophoblasts invade into the decidua, anchoring the chorionic villus and remodel the spiral arteries. In the historic etiology of preeclampsia, spiral arteries fail to undergo artery remodelling, increasing the resistance and reducing the maternal blood delivery to the fetus. This illustration was created using BioRender.com.

As research on the heterogeneity of PE expands, there is a growing recognition that distinct clinical and molecular subtypes exist, each with differing pathophysiological underpinnings. This variability poses a major challenge in developing effective diagnostic tools and therapies that work across all patients. Work from our group and others has identified at least 3 clinically and molecularly distinct subclasses of PE using an integrated approach combining clinical data, placental histopathology, and microarray-based gene expression profiling. [33–37]

- *Subclass 1 - Maternal-mediated PE (M-PE)*: This subtype appears to result from a maternal maladaptation to pregnancy, rather than placental dysfunction. Placentas in this group are morphologically and molecularly indistinguishable from healthy controls, and gene expression profiles show no signs of stress. Clinically, these pregnancies tend to progress to term or near-term, and infants are typically appropriate for gestational age (AGA). However, mother present with hypertension and often have a history of cardiovascular abnormalities, including chronic hypertension.[33,35–37] This suggests the pathogenesis may lie primarily in maternal vascular or endothelial dysfunction, independent of placental insufficiency.
- *Subclass 2 - Hypoxia-mediated PE (H-PE)*: This subclass represents the canonical for of PE that aligns with the historical two-stage model. These patients show clear signs of utero-placenta malperfusion, with placental histology revealing infarcts, reduced villous branching, increases in fibrin deposition and numerous syncytial knots - hallmarks of impaired blood supply and compromised gas and nutrient exchange.[33] Gene expression profiles are enriched for hypoxia- and oxidative stress–related pathways, indicating placental hypoxia as a central driver.[33,34,36] Clinically, this subtype is associated with early-onset PE, severe maternal hypertension, and often preterm delivery, highlighting its more aggressive disease course.

- *Subclass 3 – Inflammation-mediated PE (I-PE)*: The third subclass, representing approximately 15-20% of PE cases, is characterized by chronic inflammation at the maternal-fetal interface.[33–35] Placental histology frequently reveals inflammatory lesions, and transcriptomic analysis demonstrates upregulation of immune-related genes, including those involved cytokine signalling, viral response pathways, and markers commonly associated with allograft rejection. Despite the relatively mild maternal symptoms observed in these patients, pregnancies are often complicated by fetal growth restriction, and deliveries tend to occur in the late preterm period. This subtype underscores the possible role of immune dysregulation in PE pathogenesis, independent of classical hypoxia-driven mechanisms.

1.3 Inflammation-mediated Preeclampsia (I-PE) Subclass

1.3.1 Immune activation and cytokine imbalance

The I-PE subclass is still being actively defined, with many aspects of its physiopathology remaining unclear. However, emerging evidence suggests that this form of PE is characterized by aberrant immune activation at the maternal–fetal interface, mirroring responses typically observed in allograft rejection and foreign tissue recognition.[38,39] Histological and immunological analyses of placentas from I-PE cases have revealed increased infiltration of innate and adaptive immune cells, including $CD8^+$ T cells, $CD68^+$ macrophages, monocytes and myeloperoxidase (MPO)-positive neutrophils.[40,41] These immune populations are typically associated with pro-inflammatory responses, antigen processing, and tissue damage.

Multi-omics profiling—including transcriptomics, proteomics, and metabolomics—has identified elevated levels of pro-inflammatory cytokines in placental tissue, particularly tumour-necrosis

factor alpha (TNF-α), interleukin (IL)- 6 and IL-17.[38] In contrast, anti-inflammatory cytokines such as IL-10 and IL-4 are often reduced, further skewing the immune environment toward inflammation and immune dysregulation.[38,42,43] This imbalance likely contributes to impaired immunotolerance and placental dysfunction. In particular, TNF-α plays a central role in orchestrating the inflammatory response in I-PE.[35] It promotes upregulation of endothelial adhesion molecules, increase vasculature permeability, and facilitates recruitment of leukocytes and other immune cells to the decidua and placental bed. [35,41,43] Sustained TNF-α signaling can also activate apoptotic and necrotic pathways, leading to trophoblast cell death, tissue injury, and release of placental debris into the maternal circulation—further amplifying systemic inflammation. [22,41] Although TNF-α activity is normally present and tightly regulated during healthy pregnancy, its dysregulation in I-PE appears to disrupt the delicate immunological balance required for fetal development. However, direct TNF-α inhibition poses risks to fetal growth and immune maturation, as TNF-α also plays important roles in placental morphogenesis and immune modulation.[44] Consequently, targeting downstream effectors or signalling pathways activated by TNF-α , rather than the cytokine itself, may offer a safer and more effective therapeutics strategy.

1.3.2 Oxidative stress and ROS Production

Oxidative stress is a hallmark feature of PE and results from an imbalance of pro- and antioxidant systems during gestation.[27,38,45] One consequence of oxidative stress is the excessive accumulation of reactive oxygen species (ROS), highly reactive molecules capable of damaging cellular structures and impairing critical physiological functions.[46,47] Under normal physiological conditions, low levels of ROS are essential for healthy pregnancy. [45,48,49] They act as cellular signalling molecules, playing a role in processes such as trophoblast differentiation, angiogenesis,

and feto-placental vascular development. [50–52] For example, ROS are involved in the activation of vascular endothelia growth factor (VEGF), promoting blood vessel formation in the developing placenta and fetus, and modulate MAPK signalling pathways, which contribute to proper trophoblast invasion and placental morphogenesis. [52–54] These roles are tightly regulated by endogenous antioxidants (e.g. glutathione, superoxide dismutase, catalase), which help maintain redox homeostasis.[45,48,55–57]

However, in the context of PE, this balance is disrupted. Antioxidant levels are significantly reduced, tipping the redox environment toward a pro-oxidant state.[27,48,58] This leads to excess ROS accumulation, which not only amplifies placental inflammation – by enhancing cytokine signalling and leukocyte activation – but also contributes to a vicious cycle of cellular damage and dysfunction. [45,56,58–60] At high concentrations, ROS can damage key cellular components including lipids (via lipid peroxidation), proteins (via carbonylation) and DNA (via oxidative base modifications).[57,61–65] A well-established marker of oxidation DNA damage is 8-oxoguanine (8-oxo-dG), formed by the oxidation of guanine bases. This lesion has the propensity to mis pair with adenosine instead of cytosine during DNA replication, resulting in point mutations and genomic instability.[66–69] The placenta, with its high metabolic activity and sensitivity to oxygen fluctuations, is particularly vulnerable to ROS-induced injury. Accumulation of DNA damage and lipid peroxidation products in placental cells can trigger apoptotic and necrotic pathways, leading increased shedding of trophoblast debris into the maternal circulation. This contributes to the systemic inflammatory response and further compromises placenta health and function.[70–73] Thus, while ROS serve vital roles in early placental development, their dysregulated production in

I-PE exacerbates inflammation, promotes tissue injury, and may be a key driver of placental insufficiency in this subclass.[5,31,43]

1.3.3 Mitochondrial damage in I-PE patients

The placenta supports a range of energy-intensive functions during pregnancy, many of which are dependent on healthy mitochondrial activity. [34,74,75] As in other tissues, mitochondrial integrity in the placenta is closely linked to cellular health, and disruptions in mitochondrial function have been implicated in placental dysfunction and fetal compromise in PE.[34,60,74–77] In PE, studies have reported several indicators of mitochondrial damage compared to healthy pregnancies. These include swollen mitochondria, fragmentation of the mitochondrial network, and irregular cristae structure.[34,75,78–81] Processes responsible for maintaining mitochondrial homeostasis - such as fission and fusion dynamics - appear to be dysregulated, impairing the placenta's ability to respond to environmental stressors.[82–84] This impairment can trigger mitochondrial stress signalling, leading to the activation of mitophagy and increased expression of autophagy-related markers. [75,80,85]

Interestingly, mitochondrial content in PE placentas remains an area of active debate. Some studies report increased mitochondrial biogenesis, evidenced by elevated expression of PGC-1α (a key regulator of mitochondrial biogenesis), as well as higher mtDNA copy numbers is both early- and late-onset PE compared to controls. [34,60,76,86,87] These findings suggest a possible compensatory response to mitochondrial injury and ROS overproduction. Conversely, other reports describe reduced mitochondrial content with downregulated expression of PGC-1α, particularly in early-onset PE, implying impaired mitochondrial replication.[82] These opposing

results may reflect biological heterogeneity within PE cases, including differences in disease severity, gestational age at onset, and maternal-fetal factors. Emerging research also suggest that fetal sex and maternal hormone levels may influence mitochondrial dynamics in PE.[88–92] For instance, elevations in testosterone levels in maternal circulation during the third trimester have been associated with downregulation of PGC-1α and suppression of mitochondrial biogenesis in PE pregnancies compared to healthy control pregnancies. [91,93] Interestingly, increased mtDNA copy number has been observed in specifically placentas from female fetuses, indicating a potential sex-linked regulatory mechanism.[76,94]

These findings highlight a broader challenge: the lack of subclass-specific analysis in many prior studies. I-PE, with its unique inflammatory and immunological profile, may exhibit distinct mitochondrial adaptations compared to hypoxia-driven or maternal-mediated subtypes. Furthermore, mitochondrial phenotypes may be influenced by factors such as timing of disease onset, clinical severity, trophoblast subtype, model system used, and gestational stage at sampling. [34,95–97] In sum, mitochondrial dysfunction is likely a central contributor to placental pathology in PE. However, the direction and magnitude of mitochondrial responses remain incompletely understood within I-PE specifically, and may differ across PE subclasses, emphasizing the need for more targeted and stratified research approaches.

1.4 A PARP – SIRT Tug of War - NAD^+ Consumption in Health and Disease

1.4.1 The family of Poly (ADP) – Ribose Polymerases (PARP)

Poly (ADP) Ribose Polymerases (PARPs) are a group of enzymes that are involved in multiple cellular processes like DNA repair pathways, chromatin remodelling, metabolism regulation and apoptosis regulations[98–102]. PARPs catalyze the transfer of ADP-ribose units, often in the form of linear or branched poly – (ADP-ribose) chains, onto target proteins, in a process called PARylation.[98,98–100,102,103] PARPs use nicotinamide adenine dinucleotide (NAD^+) as a substrate for each of the ADP-ribose unit transferred, collectively serving as a predominant cellular NAD^+ consumer. The PARP family of enzymes consists of 17 members, with 4 demonstrating PARylating capabilities.[100] These poly-ADP-ribose chains added to PARylated proteins are heterogenous in length, up to 200 ADP units in length – and can be linear or branched.[104]

The remaining of enzymes only transfer one unit of ADP-ribose, in a process called MARylation (Mono-ADP-Ribosylation).[99,100] The targets of MARylation and PARylation depend on the specific cellular pathway activated by PARPs. There are over 9000 targets of PARPs with over 14,000 different target sites found since 1975, which a majority of being PARylated.[105,106] Additionally, in certain circumstances PARPs are able to auto-PARylated/MARylate themselves when activated to physically dissociate itself from the DNA repair site or the catalytic domain of the target protein.[99,101] In the context of inflammation, PARP-1 is auto-PARylated to facilitate its removal from the catalytic domain of inflammatory transcriptional complexes to further allow the expression of and downstream effects.

The most widely studied of the PARP enzymes is PARP-1, as it is the most abundantly expressed and active in human cells.[103] In these cells, PARP-1 is rapidly activated at sites of single-stranded or double-stranded DNA breaks/base excision repair, responding by PARylating itself, nuclear targets or other recruiting proteins.[103,107,108] PARP-2, one of the isoforms and the second most active PARP, is also activated in responses to cellular stress and metabolic regulation.[109–112] Tankyrase (TNKS) 1 and TNKS-2 (also known as PARP-5a and PARP-5b) are the last two PARPs with PARylation activity that are involved in telomere maintenance, WNT signaling, glucose metabolism and multiple other cellular processes.[113,114] While double knockout of *Parp-1* and *Parp-2 in* mice results in very early embryonic lethality, single knock outs of either gene produce viable animals but mild abnormalities.[112] These results are also common in *Tnks-1* and *Tnks-2* knockout mice.[115] This indicates the important of the function of PARPs and PARylation in fetal development.[112,115]

1.5 Overactivation of PARPs Across disease

PARP-1 is responsible for over 85% of any PARylation activity and its dysfunction – primarily in the form of unregulated over-activation – contributed to many diseases, including cancers, obesity cardiovascular, chronic inflammatory, and neurodegenerative diseases.[99,116] Upon hyper-activation of PARP, rapid intracellular NAD^+ depletion is noted, with consequences for other downstream NAD^+-dependent cellular functions. For example, intracellular NAD^+ depletion can lead to energy failure and cell death in neurons.[107] The mechanism behind this is controversial, with some studies suggesting a direct, NAD^+-dependent deficit in ATP production[117,118], while others suggest compromised NAD^+-dependent Sirtuin activity, and subsequent mitochondrial dysfunction.[119] Various studies have shown that PARP-1/2 inhibition or NAD^+ replenishment,

through NAD^+ precursors like vitamin B3, can rescue the potential negative effect of elevated PARP activity.[120–123] Interestingly, the role of PARPs and NAD^+-metabolism in placental disease has not yet been elucidated.

1.5.1 PARP inhibitors

PARP inhibitors (PARPi) have been investigated for over 20 years as potential therapeutic strategies for many diseases.[124] PARPi have been primarily used to target and inhibit PARP activity in different cancers such as breast, ovarian and prostate.[125–127] For example, PARPi can selectively target cancer cells with BRCA1/2 mutations by blocking PARP-dependent single-strand break repair. In the absence of functional BRCA1/2-mediated homologous recombination, unrepaired breaks accumulate and collapse into lethal double-strand breaks, a concept known as synthetic lethality.[124,125,127] Olaparib is a PARP-1/2 inhibitor that has shown significant potential to target BRCA-mutated cancers, becoming the first PARPi drug approved for treatments for BRCA-mutated ovarian cancers.[125–128] Several others have been approved since then, including Niraparib, Rucaparib and Talazoparib.[129] Generally, approved PARPi's are capable of inhibiting ~ 90% of the cellular PARylation activity. However there are a couple PARP enzymes capable of PARylation that are not inhibited by these broad spectrum inhibitors - notably TNKS-1/2 - whose inhibitors appear to target Wnt/β-catenin signalling in several types of cancers.[130–132] Wnt/β-catenin signalling is an essential cellular processes such as cell proliferation and survival.[130,131] XAV939, is a selective TNKS-1/2 inhibitor that has been studied in inflammatory diseases and cancers.[133] Interestingly, recent studies using in-vivo and in-vitro models of PE indicate that TNKS-1/2 inhibition impairs trophoblast proliferation and migration capabilities through Wnt/β-catenin signalling , suggesting an important role for Tankyrase activity in healthy placental development and function.[134]

1.5.2 NAD⁺ pathways and homeostasis

NAD^+ is a cellular co-factor that plays a role in energy metabolism, DNA repair and cellular redox homeostasis, amongst other cellular metabolic processes [135,136] In energy metabolism NAD^+ acts as an essential electron acceptor and is reduced to NADH in redox reactions at multiple steps during glycolysis and the tricarboxylic acid (TCA) cycle.[137,138] Within the ETC, Complex I oxidizes NADH molecules back into NAD^+, transferring the electrons to ubiquinone (CoQ). CoQ will then transfer the collected ETC electrons and transfer them to complex III **(Figure 2)**. Complex III is responsible for transporting electrons into the intermembrane space, creating a proton gradient capable of pumping protons into the intermembrane space and drive the ATP synthase to create ATP production.[137] As a result, alterations in energy metabolism brought on by disease or diet can alter NAD^+-homeostasis, by altering NAD^+/NADH ratios, often leading to the accumulation of NADH and the reduction in ATP production, creating a shift in cellular energy metabolism **(Figure 2)**.[139,140] Outside of redox reactions, NAD^+ is consumed as a substrate of two primary enzyme families, including PARPs and SIRTs. Importantly, consumption of NAD^+ results in the production of nicotinamide (NAM), which can be recycled through the salvage pathway to regenerate intracellular NAD^+ stores. Under normal conditions, the salvage pathway is used to help maintain NAD^+ stores.[138] The maintenance of intracellular NAD^+ levels also relies on the biosynthesis pathways: the *de novo pathway*, in which dietary tryptophan (Trp) is converted to NAD^+; and the *Preiss-Handler pathway*, which makes use of dietary nicotinic acid (NA) in the generation of NAD^+.[137] NAD^+ precursors, including NA, NAM and nicotinamide riboside (NR), are forms of vitamin B3 that can be utilized by the biosynthetic or salvage pathways to create NAD^+, and as

such have been investigated as therapeutic treatments to restore intracellular NAD^+ stores under conditions of heightened cellular stress, such as aging and disease.[120,141,142]

1.5.3 NAD^+ Depletion and Outcomes

Cellular NAD^+ levels play an essential role in many biological processes, where NAD^+ homeostasis is highly sensitive to cellular stress and can change the directions and outcomes of energy metabolism or signalling pathways that rely on NAD^+. In a wide range of diseases, NAD^+ depletion is established secondary to hyper-activation of NAD^+ consuming enzymes, ultimately compromising cellular health.[137] PARPs and SIRTs are the two most well-studied families of NAD^+-consuming enzymes that both rely on sufficient intracellular NAD^+ stores to carry out their enzymatic function. As a result, PARPs and SIRTs compete for intracellular NAD^+ stores. Notably, some PARP family members, such as PARP-1, have a higher affinity for NAD^+ compared to SIRTs, enabling them to function at lower NAD^+ concentrations.[143] Consequently, PARP activity can remain relatively unaffected in low NAD^+ conditions, while SIRT activity and its downstream effects may be compromised.[143]

1.5.4 The Protective Role of SIRTs

Sirtuins are a family of proteins that are generally responsible in the deacetylation of target histones and proteins.[144] In humans, sirtuins comprise of seven different homologs (SIRT-1 – SIRT-7) that differ in their enzymatic activities, target proteins and subcellular localization.[144] SIRTs are essential in many cellular metabolic processes and play a protective role in cellular homeostasis in response to inflammation, oxidative stress or metabolic disruptions. SIRT-1 is the most extensively studied SIRTs, as it is highly active across a broad range of pathways involved in

metabolism, stress responses, inflammation and aging – including those relevant to placental development and function. SIRT-1 plays an essential role in placental trophoblast differentiation and stem cell maintenance, in fact, SIRT-1 knockout (KO) mouse exhibit smaller placentas, structural deficits, and trophoblast differentiation impairment.[145,146] Importantly, SIRT1 expression and activity is highly sensitive to pro-inflammatory environments, adversely impacting critical downstream SIRT-1-mediated regulatory functions.[147,148] In humans, SIRT-1 activity is reduced in the serum of PE patients and the human umbilical vein endothelial cells, suggesting that circulating factors found in the serum are preventing the protection role of SIRT-1 in PE.[149,150] Considering the heightened inflammation observed at the maternal-fetal interface in the I-PE subclass, the impact of compromised SIRT-1 activity in the observed placental dysfunction observed is of interest.

One such SIRT-mediated regulatory function of considerable interest is the maintenance of mitochondrial health and function. SIRT-3, SIRT-4 and SIRT-5 are mainly localized to the matrix of the mitochondria, where they play important regulatory roles in mitochondrial biogenesis and function – ultimately being intimately involved in the regulation of both ATP and ROS production.[144,151] In accordance, several SIRT agonists (i.e. SRT2104 and SRT1720) are known to dramatically improve mitochondrial biogenesis and function.[152–154] Similarly to the use of SIRT1 agonists, PARP-1 inhibitors and *Parp1* knockout mice models have in some cases been associated with improved mitochondria biogenesis, ATP production, increased SIRT activation, and importantly, protection against metabolic diseases due to elevated NAD^+ levels.[155–158]

Together, these findings emphasize this tug-of-war in between PARPs and SIRTs over the limited availability of NAD^+, where inhibiting the activity of PARP can increase NAD^+ availability, thus increasing SIRTs activity and its downstream functions.[136,155]

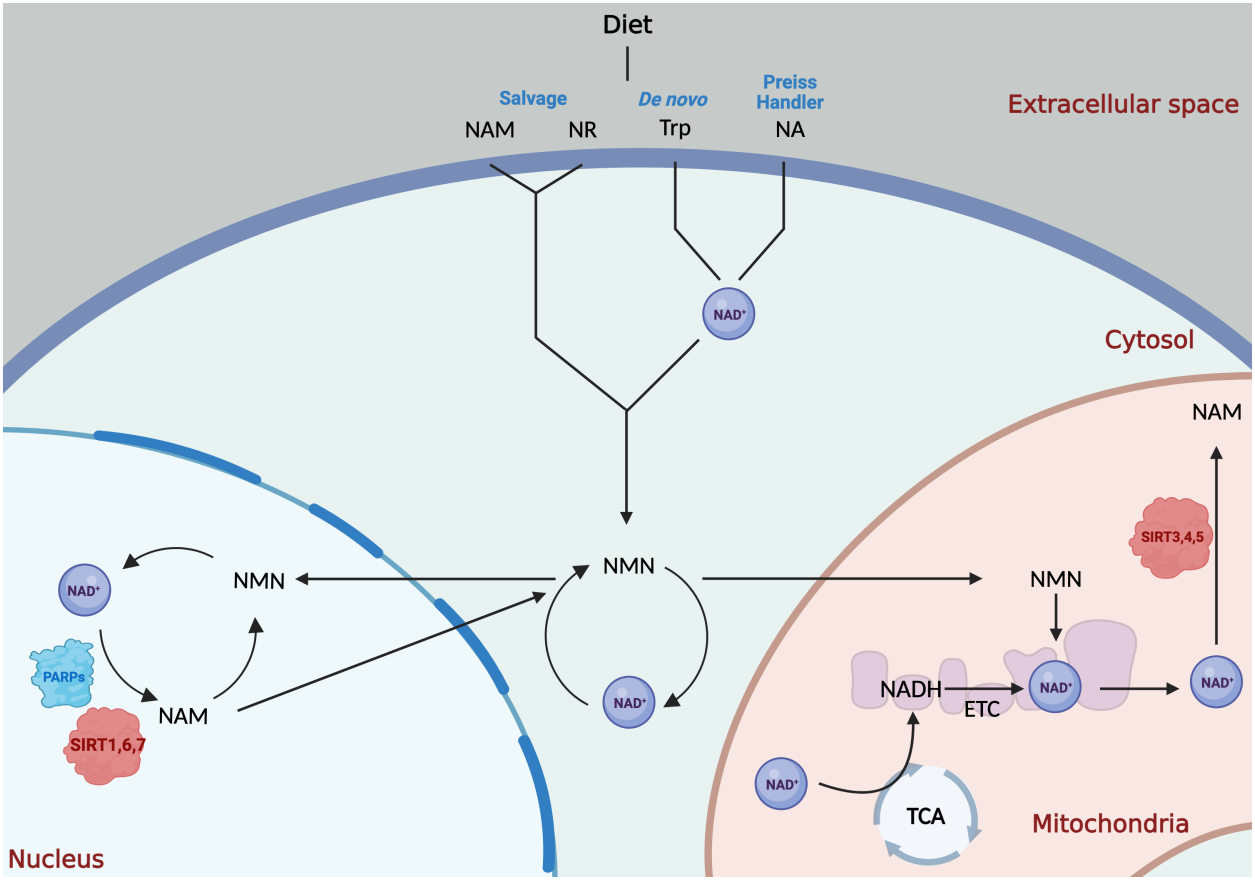

Figure 2. NAD+ metabolism and synthesis pathways. NAD^+ homeostasis is maintained by both the metabolism and the biosynthesis of NAD^+ through dietary consumption or pre-existing precursors including nicotinamide (NAM), nicotinamide riboside (NR), tryptophan (Trp) and nicotinic acid (NA). Precursors, NAM and NR are metabolized through the salvage pathway, synthesizing nicotinamide mononucleotide (NMN) that can be subsequently converted to NAD+. Trp and NA can be metabolized into NAD^+ through the De novo and Preiss Handler pathways respectively. NMN and NAD^+ can be recycled in the cytosol, nucleus and the mitochondria for the consumption of NAD+ by PARPs (nucleus) and SIRTs (found in nucleus and mitochondria), leaving NAM as a by-product. In the mitochondria, NAD^+ is reduced into NADH during glycolysis and TCA cycle, prior to oxidation in the electron transport chain (ETC). This illustration was created using BioRender.com.

1.6 NAD^+ depletion in I-PE

1.6.1 NAD^+ Boosting Strategies in I-PE

Recent work from our group, led by Jahan et al, demonstrated that there was a unique phenotype found in human placentas with I-PE, along with placenta collected from our rodent model of I-PE caused by the overactivation of PARPs. [120] Using an LPS-induced inflammation rodent model of PE, demonstrates that the pro-inflammatory response led to a reduction in placental weight, fetal weight, NAD^+ depletion and increased PAR levels.[159] Using an NAD^+ replenishing boost (NR supplement), was able to prevent hypertension, fetal growth restrictions (FGR), reduced mitochondrial health, lower oxidative stress and improvement the overall function and health. Collectively, these findings suggest that using an NAD+ supplement could be a promising therapeutic strategy for patients with I-PE.[120] However, the exact mechanism of how this inflammatory response leads to a rapid NAD^++ depletion resulting in poor placenta health is not known.

2 Hypothesis and Research Aims

Inflammation-mediated PE (I-PE) is a molecular subclass of PE characterized by chronic placental inflammation, excessive protein PARylation, NAD^+ depletion and mitochondrial dysfunction **(Figure 3)**. These metabolic and functional impairments appear to reduce placental efficiency and contribute to fetal growth restriction. Although PARP-1/2 and TNKS-1/2 enzymes are the principal NAD^+-consuming PARylating enzymes which are known to become highly activated under inflammatory stress, their individual contributions to these pathogenic features remain undefined. Addressing this gap is essential to pinpoint mechanisms linking inflammation to placental dysfunction. By integrating cross-model comparisons (human placenta, a rodent model of I-PE, and trophoblast cell culture) with both expression profiling and targeted enzyme inhibition, this study will define the roles of PARP-1, PARP-2, TNKS-1, and TNKS-2 in trophoblast dysfunction. Together, these approaches increase translational relevance and may identify the PARP–NAD^+ axis as a therapeutic target in I-PE.

Hypothesis:

PARylating enzymes (PARP-1, PARP-2, TNKS-1, TNKS-2) in I-PE drives NAD^+ depletion and mitochondrial dysfunction, leading to impaired trophoblast function, and thereby contributing to placenta insufficiency.

Aims:

This hypothesis will be tested through the completion of the following research aims:

AIM 1 – Profile the mRNA expression and activity of key NAD^+-consuming PARylating enzymes (PARP-1, PARP-2, TNKS-1 and TNKS-2) in placental tissue from I-PE cases, a rodent model I-PE, and TNF-α–stimulated trophoblasts in vitro.

AIM 2 – Determine the functional consequences of selectively inhibiting PARP-1, PARP-2, TNKS-1 and TNKS-2 on protein PARylation, mitochondrial function, cell viability, and trophoblast migration in TNF-α stimulated HTR-8/SVneo cells in vitro.

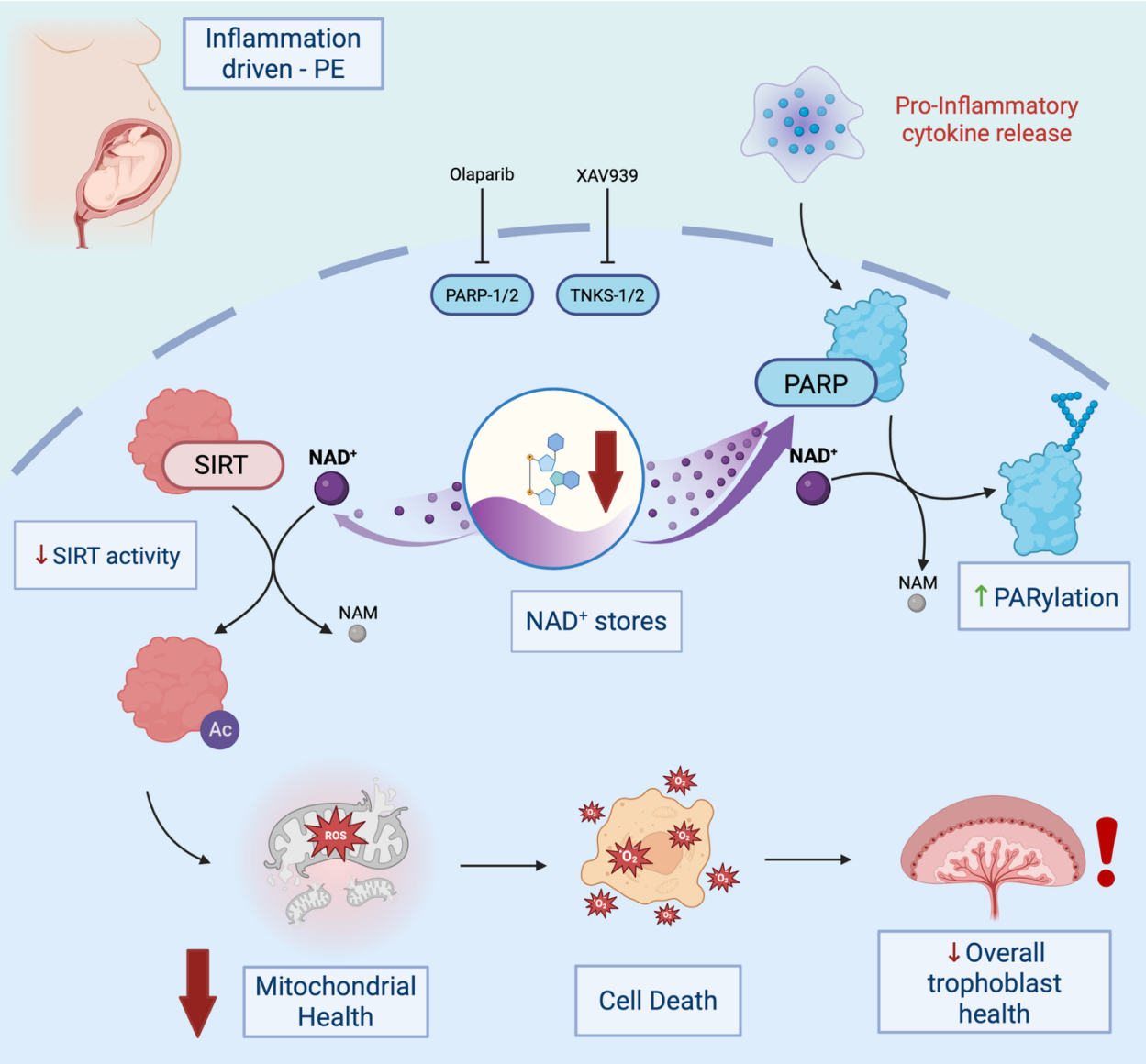

Figure 3. Role of PARPs and dysregulated placental NAD+ signaling in the inflammation-driven subclass of preeclampsia. A pro-inflammatory response in the placenta leads to an increase in PARP activity, leading to excessive PARylation. PARPs and SIRTs both compete for the same NAD^+ pool and under inflammation, PARPs rapidly deplete this NAD^+ availability, supressing the protective role of SIRTs deacetylation in mitochondrial health and function. This cascade leads to mitochondrial dysfunction that ultimately reduces trophoblast viability and overall, the health of trophoblasts. Olaparib and XAV939 are used to inhibit the activity of PARP that can PARylate. This illustration was created using BioRender.com.

3 Materials and Methods

3.1 Human Placenta Tissue

Frozen human placenta biopsies were obtained from Research Centre for Women's and Infants' Health BioBank (RCWIH) and previously underwent detailed molecular profiling to determine PE subclassification (University of Ottawa REB protocol# H08-17-08, Mount Sinai Hospital REB protocol# 20-0037-E).[35] Placental biopsies from healthy controls (n=23) and cases with I-PE (n=10) were identified and selected for mRNA gene expression measurements. Characteristics of each control and I-PE case is listed in **Table 1**. PE was defined as the onset of hypertension (systolic pressure > 140 mm Hg and/or diastolic pressure > 90 mm Hg) after 20 weeks of gestation coupled with evidence of maternal end-organ dysfunction. Classification of each subclass was done by microarray and histopathology analysis and confirmed by qPCR analysis, as described in Leavey et al., 2016.[35]

3.1.1 RNA Extraction and Purification

Flash frozen human placenta tissues (~20 mg) were homogenized in 500 µL of TRIzol™ with 2 ceramic beads at room temperature. Samples were homogenized in the Bead Mill 24 Homogenizer (Fisher Scientific) and homogenized for 40 seconds followed by 20 seconds of rest and repeated three times. 100 µL of chloroform was added to each sample and mixed by inversion followed by an incubation of 5 minutes to separate the phases. Samples were centrifuged for 15 minutes at 12,000 x g at 4°C. The mixture separated into the lower organic phase and interphase containing lipids, proteins and any remaining cell debris while the upper aqueous layer contained mainly RNA and DNA. The aqueous phase was extracted carefully using a pipette and transferred

into a new 1.5 mL microcentrifuge tube. The RNA was precipitated by mixing 250 µL of isopropanol to the extracted aqueous phase and incubated for 10 minutes at room temperature. The samples were then centrifuged for 10 minutes at 12,000 x g at 4°C to pellet the RNA. The supernatant was discarded, and the pellet was resuspended in 500 µL of 75% ethanol. Each sample was briefly vortexed and centrifuged for 5 minutes at 7,500 x g at 4°C. The supernant was discarded and the RNA pellet was left to air dry for 10 minutes and resuspended in 50 µL of RNase-free water.

3.1.2 RNA Quantification and Quality Analysis

The concentration of the extracted mRNA was assessed using the NanoDrop2000 Spectrophotometer, along with the mRNA quality via the A260/A280 ratios. High quality RNA exhibit ratios of absorbances at 260 nm and 280 nm of 1.9-2.0 to ensure no proteins or salt contamination were left. RNase-free water was used to blank the spectrophotometer and 1 µL of mRNA extracts was used on the Nanodrop.

3.1.3 gDNA removal and cDNA Synthesis

mRNA concentrations were normalized to 50 ng/µL in a final volume of 20 µL, and samples were prepared in 8-strip PCR tubes. To eliminate potential genomic DNA (gDNA) contamination, a DNase treatment was performed using the iScript™ gDNA Clear cDNA Synthesis Kit (Bio-Rad, Cat # 1725035). Samples were incubated with the DNA master mix at 25°C for 5 minutes, followed by DNase deactivation at 75°C for 5 minutes. Following gDNA- removal, cDNA synthesis was carried out by adding the iScript Reverse Transcription Supermix (Bio-Rad, Cat # 1708840) according to the manufacturer's protocol.

3.1.4 qPCR Analysis

The mRNA expression levels of key NAD^+-dependant PARylating enzymes were quantified using quantitative PCR (qPCR). Primer sequences used for target genes are provided in Table 1. Each qPCR reaction contained 5 µL of SsoAdvanced™ Universal SYBR® Green Supermix (Bio-Rad, Cat # 1725270), 10 µM each of forward and reverse primer, and 20 ng of cDNA per well. Reactions were performed in triplicates on a 384 well plate using the CFX384 Real-Time PCR System (Bio-Rad, Cat #1855484). Cycle threshold (Ct) values were analyzed using the ΔΔCq method, normalized to the geometric mean of YWHAZ, RNA18S and GAPDH. Relative gene expression (fold change) was calculated to compare expression levels of genes listed in Table 1.

Table 1: Characteristics of Patients

Characteristic	Control (n=23)	I-PE (n=10)
Maternal Age (years)	32.9	35.5
Gestational Age (weeks)	37.5	36.1
Fetal Sex (M)	14/23	6/10
Birth Weight (g)	3177	2493
Placental Weight (g)	601.8	466.6
Mode of delivery (Vaginal)	8/23	1/10
Maximum Systolic Blood Pressure (mm Hg)	116.6	138.1
Maximum Diastolic Blood Pressure (mm Hg)	75.0	86.0

3.2 Rat Placenta Tissue

Previously collected flash frozen placenta tissue from Sprague Dawley Rats was used for this study, including samples from the lipopolysaccharide (LPS) -induced inflammation-mediated PE group (n=8) and saline-treated controls (n=8) from our previous study conducted by one of our previous lab members.[120] To induce inflammation, rats were administered intraperitoneal injection of LPS every other day from gestational day (GD) 13 to GD18 at escalating doses ranging from 20 to70 µg/kg/day. On GD19, pregnant dams were sacrificed, and placentas were collected and immediately flash frozen for downstream analysis.

3.2.1 mRNA Expression Measurements

The flash frozen placenta samples were prepared as described in 3.1.1 to 3.1.3 and mRNA expression measurements were performed as described in 3.1.4. Primer sequences used for target genes are provided in Table 2. Cycle threshold (Ct) values were analyzed using the ΔΔCq method, normalized to the geometric mean of YWHAZ, RNA18S, B-ACT.

3.2.2 Protein Extraction and Preparation

Approximately 20 mg of frozen placenta tissue was homogenized in 10 µL/mg of prepared radioimmunoprecipitation (RIPA) buffer, supplemented with Roche Complete Protease Inhibitor (0589297001, Roche Canada), Roche PHOStop Phosphatase inhibitor (04906837001, Roche Canada), Tannic acid (100 µM), Olaparib (1 µM), TSA (1 µM), and Sodium butyrate (5 mM). Three 2.8 mm ceramic bead were added to each tube, and samples were homogenized at 2000 rpm for 45 seconds using the Bead Mill 24 Homogenizer (Fisher Scientific), for up to 3 cycles. Homogenized samples were then centrifuged at 16, 000 r.p.f for 10 minutes at 4°C. The

supernatant was collected for downstream analysis, and the pellet was discarded. Final lysates were stored for subsequent protein quantification.

3.2.3 Protein Quantification and Preparation

Protein concentrations were quantified using the DC protein assay, a colorimetry assay based on the Lowry method. A bovine serum albumin (BSA) stock solution (2 g/L) was freshly prepared in RIPA buffer and serially diluted into 7 standard concentrations ranging from 0 to 2000 mg/mL for the standard curve. All standards and protein samples were read in triplicate at 750 nm using a POLARstar Omega plate reader (BMG Labtech). Protein concentrations were calculated by applying the sample absorbance values to the linear regression equation generated using the BSA standard curve. All protein lysates were subsequently adjusted to 1 µg/µL by dilution with RIPA buffer. For downstream applications, samples were prepared by adding 4X Laemmli buffer, in a 1:4 ratio (sample: buffer), and 10% β-mercaptoethanol.

3.2.4 SDS-PAGE and Blot Transfer

Prepared protein samples were denatured by heated at 95°C for 5 minutes, unless specified otherwise. Proteins were separated using 4-12% gradient acrylamide SDS-PAGE gels, selected based on the molecular weight of the target protein. Gels were prepared one day prior using TGX Stain-Free FastCast Acrylamide Kit (Bio-Rad, Cat# 1610183) with 10% ammonium persulfate (APS), cast using a 1.5 mm Mini-Protean gel caster system (Bio-Rad, Cat# 1658006FC) and stored at 4°C. Each gel included 8 µL of Precision Plus Protein™ All Blue Prestained Protein Standards (Bio-Rad, Cat#1610373). Protein lysates (10-30 µg per well) were loaded based target protein

abundance. Electrophoresis was carried out at 90 V for 20 min, followed by 120 V for 60 min, or until optimal separation of the protein ladder was achieved.

Following electrophoresis, stain-free polyacrylamide gels were activated for 45 seconds using the Stain-Free Activation setting on the ChemiDoc Touch Imaging System (Bio-Rad). Proteins were then transferred onto a 0.45 mm nitrocellulose membrane using the Trans-Blot Turbo System (BioRad), with the 1.5 mm gel setting, and two stacks of ion-reservoir filter paper on each side. Membrane was imaged post transfer using the Stain-Free Blot setting on the ChemiDoc Touch Imaging system (Bio-Rad) to ensure complete transfer of protein. Membranes were then blocked in 5% w/v bovine serum albumin (Sigma, SKU A7906) diluted in TBS-T and incubated at room temperature with gentle shaking (100 r.c.f.) or one hour.

3.2.5 Immunoblotting

Following blocking, membranes was quickly rinsed with TBS-T and incubated overnight at 4°C with the appropriate primary antibody, diluted in 10 mL of 5% w/v BSA in TBS-T, in a slow-shaking incubator. The following day, membranes were washed once with TBS-T, then incubated for one hour at room temperature with the corresponding horseradish peroxidase (HRP)-conjugated secondary antibody, diluted in 5% w/v BSA in TBS-T. Following the incubation, membranes were washed three times for 5 minutes each with TBS-T on the shaking incubator at room temperature. Protein bands were visualized using a 1:1 mixture of Clarity Western Peroxide Reagent and Clarity Western Luminol/Enhancer Reagent (Bio-Rad, 1705061), or Clarity Max (Bio-Rad, 1705062S) when signal detection was weak. The membrane was then covered with the ECL mixture and imaged using the ChemiDoc Touch Imaging system (Bio-Rad) with automatic exposure settings

adjusted for optimal signal clarity. Details of all primary and secondary antibodies used are listed in **Table 3**.

3.2.6 Densitometry Analysis

Semi-quantitative densitometry analysis of protein expression was performed using ImageLab software (Bio-Rad). The intensity of the immunoreactive bands corresponding to the protein of interest was measured and normalized to the total protein signal from the stain-free blot image.

3.3 Cell Culture

HTR-8/SVneo cells, an immortalized trophoblast cell line derived from first-trimester human chorionic villi explants, were purchased from ATCC (CRL-3271) and used as an in vitro model of placental development and function. HTR-8/SVneo cells were maintained as describe in **Figure 4**. HTR-8/SVneo cells were cultured between passages 2-25 in RPMI-1640 medium (Wisent, Cat# 350-000) supplemented with 10% fetal bovine serum (FBS) and 1% Penicillin Streptomycin (P/S) at 37°C, 5% CO_2, 20% O_2 prior to one of the following experimental treatments.

1. Vehicle control - 0.1% DMSO
2. Pro-Inflammatory insult - 10 ng/uL TNF-α.
3. Inhibition of PARP 1/2 - 3 uM Olaparib.
4. Inhibition of PARP 1/2 + pro-inflammatory insult - 3 uM Olaparib + 10 ng/uL TNF-α.
5. Inhibition of TNKS 1/2 - 10 uM XAV939
6. Inhibition of TNKS 1/2 + pro-inflammatory insult - 10 uM XAV939 + 10 ng/uL TNF-α.
7. Inhibition of PARP 1/2 and TNKS 1/2 - 3 uM Olaparib + 10 uM XAV939

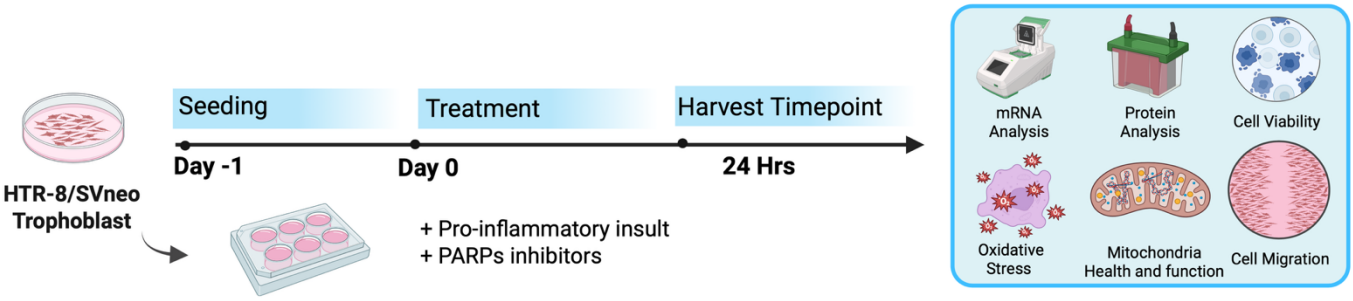

Figure 4. HTR-8/SVneo Model of I-PE. HTR-8/SVneo trophoblast used as a model of specialized extravillous trophoblast cells (EVTs) in the placenta. HTR-8/SVneo cells were seeded for 24 hours, prior to switching the media to different experimental treatments including a pro-inflammatory insult alone and combined with PARP inhibitor to investigate the role of PARP-1/2 and TNKS-1/2 in I-PE. After 24 hours, HTR-8/SVneo cells were harvested for the different cellular assessment listed.

3.3.1 mRNA Expression Measurements

HTR-8/SVneo cells were seeded at a density of 2.5 x 10^5 cells/well in 6-well plates and allowed to adhere for 24 hours. Following adhesion, media was replaced with the experimental treatments and placed in the incubator for an additional 24 hours. After treatment, cells were rinsed once with PBS, and total RNA was extracted using the EZ-10 DNAaway RNA Miniprep Kit (BioBasic, Cat# BS88133) as described in the manufacturer's protocol. The cDNA synthesis and downstream qPCR analysis were performed as described in *3.1.2.* to *3.1.4*. Gene expression was quantified using primers listed in **Table 2** and normalized to the geometric mean of YWHAZ, RNA18S, GAPDH.

3.3.2 Protein Expression Measurements

HTR-8/SVneo cells were seeded at a density of 2.5 x 10^5 cells/well in a 6-well plate and allowed to adhere for 24 hours prior to switched the media to the experimental treatments. After 24 hours of treatment, cells were washed with PBS 2x, followed by the addition of 200 µL of RIPA buffer supplemented with the following: Roche Complete Protease Inhibitor (0589297001, Roche Canada), Roche PHOStop Phosphatase inhibitor (04906837001, Roche Canada), Tannic acid (100

µM), Olaparib (1 µM), TSA (1 µM), and Sodium butyrate (5 mM). Tannic acid was used to inhibit dePARylating activity by poly - (ADP) ribose glycohydrolase (PARG), Olaparib was used to inhibit PARylating activity from poly- (ADP) ribose polymerases (PARPs), and lastly sodium butyrate to inhibit the activity from histone deacetylases (HDAC). Protein lysates were subjected to three freeze-thaw cycles, then sonicated on ice using three 10-second pulses with 20-second intervals between each to prevent overheating. Samples were then centrifuged at 16, 000 r.p.f for 10 minutes at 4°C, and the resulting supernatant was collected for protein quantification as described in 3.2.3. Protein analysis and immunoblotting procedure were performed as detailed in sections 3.2.4 to 3.2.6., with antibodies listed in **Table 3**.

3.3.3 Mitochondrial Respiration Measurement

HTR-8/SVneo trophoblast cells were seeded at 7.5 x 10^3 cells/well in a Seahorse XFe96 plate in 80 µL of media and allowed to settle at room temperature for 2 hours to reduce edge effects. Cells were plated in 12 technical replicates per treatment condition, excluding the outermost wells to serve as background controls for the Agilent Seahorse XF Cell Mito Stress Test. After the initial 2-hour settling period, wells were topped up to 200 µL and incubated for an additional 22 hours. Following this, media was replaced with fresh media containing the experimental treatments and left for 24 hours. The sensor cartridge was hydrated overnight at 37°C in a non-CO_2 incubator and then equilibrated in calibrant solution for 4 hours prior to use. Two hours before the assay, cells were washed 3x with Seahorse XF RPMI assay media supplemented with 10 mM glucose, 1 mM pyruvate, and 2 mM glutamine (pH 7.4). Cells were maintained in 175 µL of the same media at 37°C in a non-CO_2 incubator. The baseline oxygen consumption rate (OCR) was measured using the Seahorse XF Analyzer. After baseline OCR measurement, the following compounds were

sequentially injected: Oligomycin (1.5 µM) to assess ATP-linked respiration, FCCP (1 µM) for maximal respiration, and Rotenone + Antimycin A (1 µM) to measure non-mitochondrial respiration. The final concentration of each mitochondrial complex inhibitor was optimized by using range of concentrations to ensure inhibition during the Mito Stress Test:

- Oligomycin: 0.5 – 2 µM
- FCCP: 0.5 – 2 µM
- Rotenone/antimycin A: 0.5 – 2 µM

After the assay, cells were washed once with 100 µL of PBS and lysed in 30 µL of RIPA buffer. Protein concentration was determined using the DC protein assay (BioRad) as described in section 3.2.3, and seahorse data were normalized to total protein content.

3.3.4 Migration Function Measurements

HTR-8/SVneo cells were seeded at a density of 3.0 x 10^5 cells/well in a 6-well plate and cultured until 90-95% confluency was reached. After 20 hours, the media was replaced with starvation media consisting of RPMI-1640 (Wisent, Cat# 350-000) and 1% P/S (in the absence of FBS supplementation) and incubated at 37°C, 5% CO2, 20% O2 for 5 hours. Following starvation, a scratch assay was performed by making vertical and horizontal scratches using a P200 pipette tip, followed by a PBS wash to remove detached cells. The media was then replaced with starvation media containing the appropriate experimental treatments. Images of each scratch intersection (where vertical and horizontal lines cross) were captured at 10X using the Invitrogen™ EVOS™ XL Core Imaging System (Fisher Scientific). After 24 hours, wells were washed once with PBS, and

final images were captured at the same intersection. Images processing and quantitative migration analysis were conducted as described by Ranzoni et al[160].

3.3.5 Cell Viability Measurements

HTR-8/SVneo cells were seeded at 1.0 x 10^4 cells/well in a 96-well plate and incubated for for 48 hours. Cells were plated in triplicate for each experimental treatment. Once cultures reached 50-60% confluency, cells were washed once with PBS, followed by replacement with fresh media containing the experimental treatments. H_2O_2 (0.2 uM) was added to negative control wells 30 minutes before measurement as a cytotoxicity control. After 24 hours, cells were washed twice with 1X PBS, before adding Cell Dye II/Calcein AM buffer and reading the fluorescence at Ex/Em = 485/530 nm as per the Calcein AM assay (Abcam, Cat# ab228556) manufacturer's protocol. Calcein fluorescence was quantified using POLARstar Omega plate reader (BMG Labtech).

3.4 Statistical Analysis

All data are presented as mean ± standard error of the mean (SEM) unless otherwise indicated to reflect the estimated mean across experiments. Statistical analyses were performed using Graphpad Prism (version 10; GraphPad Software). For comparisons between two groups, unpaired two-tailed student's t-test were conducted for the human and rodent results. Any comparisons made with the cell culture experiments were paired, as they were treated at the same time and from the same batch of cells. For experiments involving more than two groups, a one-way ANOVA was used, followed by Tukey's post hoc test, unless otherwise specified. Normality of the data was assessed using the Shapiro-Wilk test. A p-value ≤ 0.05 was deemed statistically significant.

Table 2: List of Primer Pairs

Species	Gene of Interest	Sequence
Human	*PARP-1*	F: TGGAAAAGTCCCACACTGGTA R: AAGCTCAGAGAACCCATCCAC
Human	*PARP-2*	F: GGCACAAATCAAGGCAGGTTA R: AAGTCATGCGGAATCCTGGTG
Human	*TNKS-1*	F: TGGATCTCTGGCAGTTTACTCC R: TCAATCTCTCCCTAAGCTCCG
Human	*TNKS-2*	F: GGGTGTCCAGTTCACAAAGA R: AAGCCTGTTCTCCTCTGTAAATAA
Human	*PARP-7*	F: ACTTTGATCCCCGTGTCTGT R: GCCCATTGTGTATCTGCCAG
Human	*PARP-10*	F: ATGACTGGCTTTCGGCTCTG R: GCACAACACATGGCAGCTAA
Human	*PARP-12*	F: GCCATGACTTACGGTGCTACC R: CCAAACTCATCACTCCAGTACCA
Human	*PARP-14*	F: CACCTGGAAGATGATGGAGCCA R: GAGGTTCACTTTCTGCTGCACC
Rodent	*Parp-1*	F: TTGACTATGGCCAGGACGAAGA R: CTGCCTTCTGCTCAGTTTCCC
Rodent	*Parp-2*	F: CCAAGGTCGGAAAGGCTCAT R: TGTGCTGCCCTGTTTTCCCA
Rodent	*Tnks-1*	F: ACGGCTCTGACCCTTCCATC R: GGCTGCACAGTTGCTTCACA
Rodent	*Tnks-2*	F: TAGCAGACCCATCCGCCAAA R: TTCTCCTCATTGCCACTCCTGG

Rodent	*Sirt-1*	F: AAGTTGACTGTGAAGCTGTACG R: TGCTACTGGTCTTACTTTGAGGG
Rodent	*Sirt-2*	F: CACGCAGAACATAGATACCCTG R: CAGTGTGATGTGTAGAAGGTGC
Rodent	*Sirt-3*	F: CCCCAAGCCCTTTTTCACTTT R: CGACACTCTCTCAAGCCCA
Rodent	*Sirt-4*	F: CCGTAGAGCTGTGAGAGAATGA R: ACCCAATGGAGGCTTTCGAG
Rodent	*Sirt-6*	F: TGTTTGTGGAAGAATGTGCCA R: CCTTAGCCACGGTGCAGAG
Housekeeping genes		
Human	*RNA18S*	F GCGGCGGAAAATAGCCTTTG R: GATCACACGTTCCACCTCATC
Human	*GAPDH*	F: AGCCACATCGCTCAGACAC R: GCCCAATACGACCAAATCC
Human	*YWHAZ*	F: TGTAGGAGCCCGTAGGTCATC R: GTGAAGCATTGGGGATCAAGA
Rodent	*B-act*	F: ATTGGCAATGAGCGGTTC R: GGATGCCACAGGACTCCAT
Rodent	*Gapdh*	F: GTGAAGGTCGGTGTGAACGG R: TGAACTTGCCGTGGGTAGAGT
Rodent	*Ywhaz*	F: GGTCATCTTGGAGGGTCGTCT R: CTGCGAAGCATTGGGGATCAA

Table 3: Primary Antibodies used in Western Blotting

Antibody	Company	Cat #
Poly/Mono-ADP Ribose antibody	Cell Signalling Technology	E6F6A
PARP1 Antibody	Santa Cruz Biotechnology	SC-8007
Total OXPHOS WB Antibody Cocktail	ABCAM	ab110413
4-hydroxynonenal Antibody	R&D systems	MAB3249

4 Results

4.1 Expression of PARPs Across Models of I-PE

Two models of I-PE were employed to compare the gene expression of PARPs relative to their respective controls. The first model consisted of human placenta samples obtained from the RCWIH Biobank, comparing placentas from I-PE cases to those from healthy pregnancies. The second model utilized an in-vivo LPS-induced model of I-PE previously established by our group, which mimics many characteristics seen in human cases of I-PE.[159] Across the two models of I-PE, the expression of MAR- and PAR-ylating PARPs was quantified and analyzed. *Parp-1* expression was upregulated in the LPS-induced rodent model but remained unchanged in human I-PE placenta samples **(Figure 5A-B)**.

Multiple RT-qPCR attempts using the human placenta samples yielded inconsistent amplification, with some reactions showing no detectable signal. This likely resulted from RNA degradation or contamination. Indeed, the RNA integrity number (RIN) for these samples was below the acceptable threshold of 7, reducing confidence in the resulting data.[161] The human placenta samples had been curated by our group more than 5 years ago, and most had undergone at least one freeze-thaw cycle during long-term storage. Consequently, we suspect that cumulative RNA degradation over time and repeated handling contributed to the compromised RNA quality observed in these specimens.

The gene expression of other PARylating PARPs and Tankyrases (*PARP-2, TNKS-1, TNKS-2)*, remained consistent and showed no significant differences across I-PE models (**Figure 5A-B**). These findings align with prior research identifying PARP-1 as the principal PARylating enzyme

mediating inflammatory responses.[99,100,120,121] MARylating enzymes (PARP-7, PARP-10, PARP-12, PARP-14) are also known contributors to inflammation; however, in our study, upregulated gene expression of these mediators was only observed in the LPS-induced rodent model **(Figure 5C)**. As noted, compromised RNA integrity limited reliable interpretation of the human biobank mRNA data. Supporting this, microarray data acquired from previous group work on these same samples (when freshly acquired) did in fact show increased gene expression of these MARylating enzymes, in a similar fashion to that observed in the LPS-induced model.[162]

To examine whether changes in *PARP* transcript expression correlated with modulation of *SIRT* genes, we focused on the LPS rodent model – the only system showing significant *Parp* transcript variation. Notably, increased expression of *Parp-1*, *Parp*-7, Parp-10, *Parp-12* and *Parp-14* was accompanied by significant upregulation in *Sirt-1, Sirt-3, Sirt-4, Sirt-6* **(Figure 5D)**. As previously described, sirtuins regulate mitochondrial function and oxidative stress responses: SIRT-3 and SIRT-4 are localized to the mitochondria, maintaining redox balance and metabolic homeostasis, whereas SIRT-1 and SIRT-6 are nuclear, governing transcriptional control of mitochondrial biogenesis and inflammatory signaling.

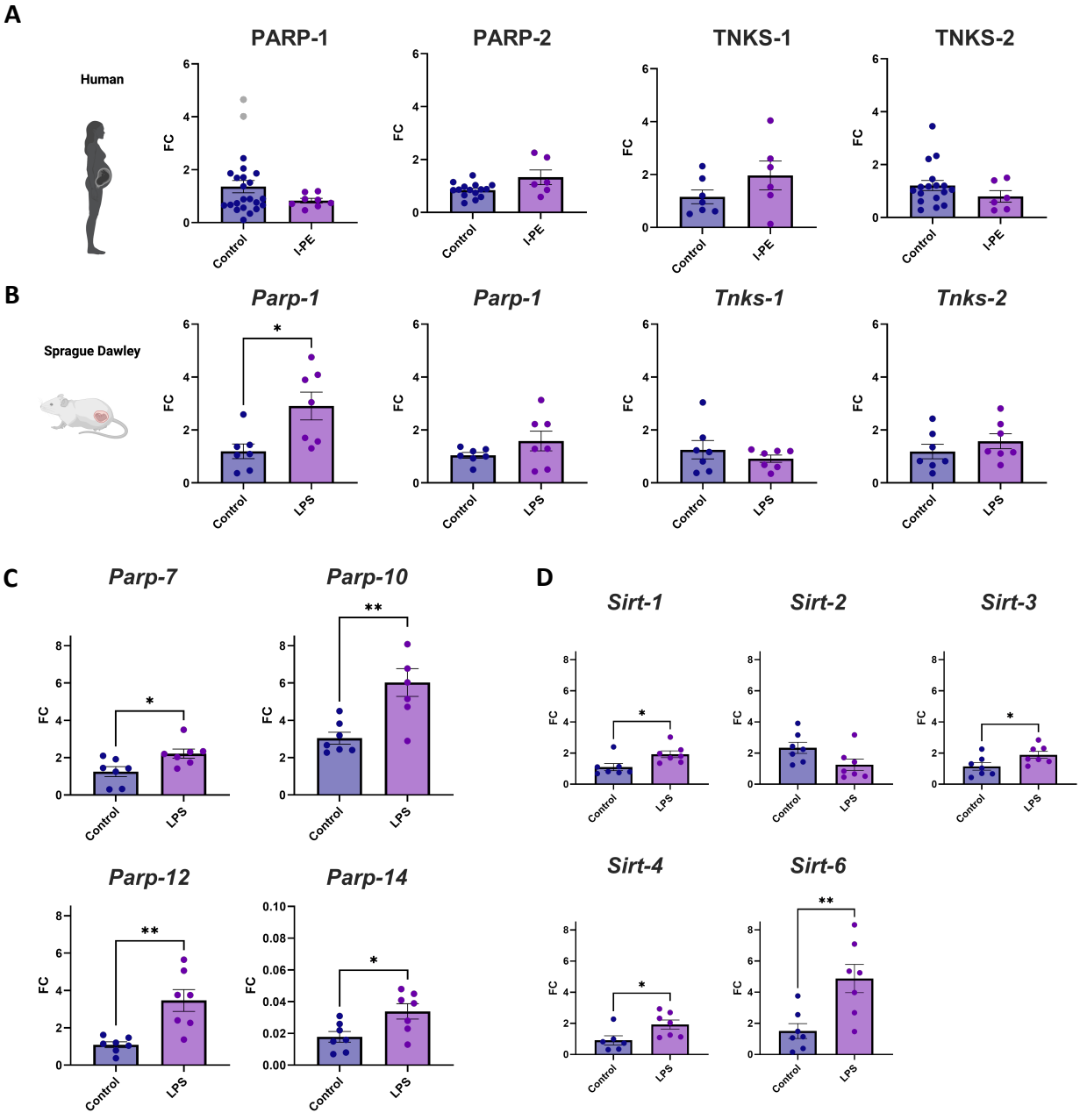

Figure 5. Expression of NAD+ Consuming Enzymes Across Models of the Inflammatory subclass of Preeclampsia (I-PE). The mRNA expression of *PARP-1, PARP-2, TNKS-1, TNKS-2, PARP-7, PARP-10, PARP-12* and *PARP-14* was measured and compared in two experimental models: i) human placenta biopsies from I-PE patients versus healthy controls and ii) an in vivo rodent model of LPS-induced I-PE compared with saline control. mRNA expression was quantified by RT-qPCR and are presented as fold change relative to controls, normalized to the geometric mean of three housekeeping genes. Summary visualization of mRNA expression changes for *PARP* and *TNKS* family members of **(A)** human placenta samples and **(B)** LPS-induced rodent model of I-PE. The

fold change in the mRNA expression of **(C)** MARylating enzymes and **(D)** SIRT family members in the LPS-models were quantified and shown. Relative mRNA expression data for these same enzymes are presented as mean ± S.E.M. across both models, with individual data points representing biological replicates. Statistical significance was determined using student's t-test where *p<0.05, ** p<0.01, ***p<0.001.

While our mRNA expression analysis provided an initial overview of transcriptional changes, the results suggest that inflammatory signaling in preeclampsia may not be primarily driven at the transcriptional level. Instead, many of the relevant regulatory events likely occur post-translationally through alterations in enzyme activity and protein modification. This aligns with current understanding that MAR/PARylation dynamics are often regulated by enzyme activation, substrate availability, and cellular stress responses, rather than by changes in PARP gene transcription.[163] Moreover, modest or inconsistent mRNA changes across models may reflect the complex interplay between transcriptional and post-translational regulation during inflammation.

Given these observations, subsequent experiments focused on the in vitro HTR-8/SVneo model, which provides a controlled system to dissect these mechanisms. Using this model allows for direct manipulation of enzyme activity through pharmacological inhibitors of PARP and related NAD^+-consuming enzymes, thereby isolating the contribution of enzymatic activity and MAR/PARylation to inflammatory signaling. This approach enables a clearer understanding of how inflammatory stress modulates PARP function and downstream cellular responses.

4.2 Confirmation of MAR/PAR inhibition with PARP Inhibitors

We next moved to examine the effects of PARP inhibition on MAR/PARylation in HTR-8/SVneo cells under inflammatory conditions. First, we wanted to confirm basal levels of MAR/PARylation

in this cell line and ensure that the enzyme inhibitors selected would work appropriately in this cell culture model.

Under basal conditions, global MAR/PAR modification levels were low, consistent with minimal PARP activation under resting conditions **(Figure 6A)**. Following oxidative stress induction (via H_2O_2 treatment) global MAR/PARylation levels were trending upwards, reflecting activation of PARP-mediated DNA damage response pathways. Treatment with the PARP-1/2 inhibitor olaparib led to a dose-dependent trend in MAR/PAR signal intensity, demonstrating inhibition of PARP-1/2 activity **(Figure 6A)**. Similarly, inhibition of TNKS-1/2 using XAV939 produced a trending decrease in global MAR/PARylation in a dose-dependent manner (**Figure 6B**). This reduction was observed even in the presence of recombinant Wnt ligand (Thermo Fisher, 120-49-20UG), which normally enhances TNKS-mediated signaling. Increasing the sample size may allow the trends to reach statistical significance. Together, our preliminary results suggest that both olaparib and XAV939 may suppress MAR/PAR formation, along with the current concentration being used in the literature to support their use as pharmacological tools for dissecting enzyme-specific contributions to inflammatory signaling in subsequent experiments.

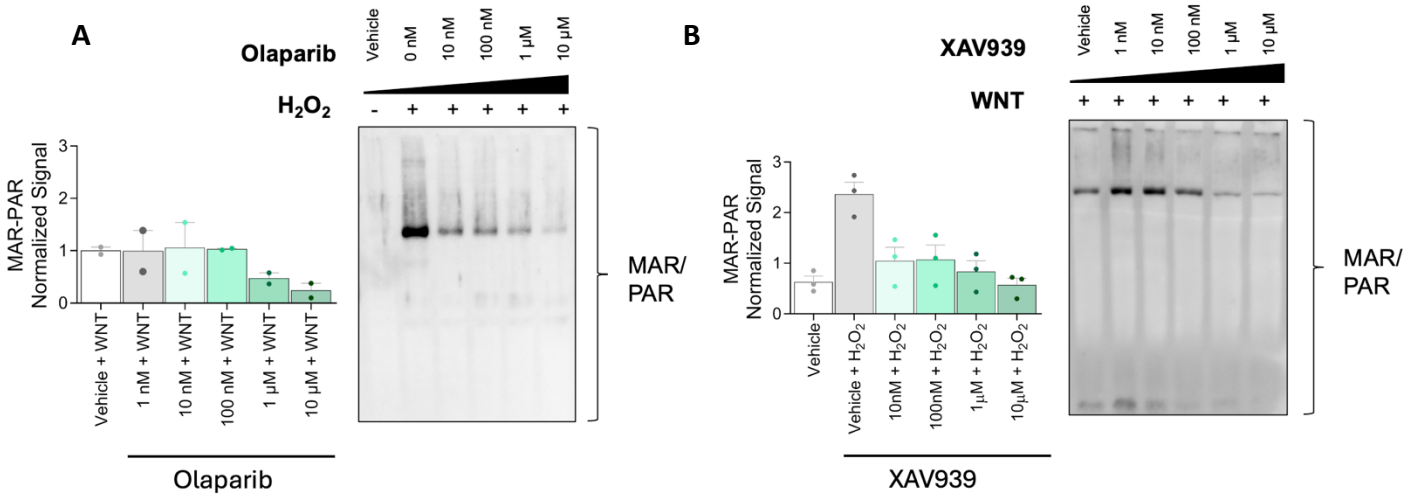

Figure 6. Validation of MAR/PAR inhibition with Olaparib and XAV939 in HTR-8/SVneo cells. HTR-8/SVneo cells were treated with increasing concentrations of (A) the PARP-1/2 inhibitor Olaparib (10 nM - 10 uM) and (B) the TNKS-1/2 inhibitor XAV939 (1 nM- 10 uM). Cells were subsequently stimulated with either H_2O_2 (0.8 mM, 30 min) or Wnt ligand (100 ng/µL, 24 h) to induce MAR/PARylation. Global MAR/PAR modifications were quantified by western blot to confirm effective inhibition of enzyme activity in a dose-dependent manner. Representative western blots (right) and corresponding densitometric analyses (left) are shown for each inhibitor. Global MAR/PAR signals were normalized to stain-free total protein. n = 2 biological replicates.

4.3 PARP-1/2 Inhibition decreases MAR/PAR Modification under TNF-α-induced Inflammatory conditions

As shown previously, global MAR/PARylation levels in HTR-/SV cell increased following TNF-α treatment *in vitro* **(Figure 7 A-B)**, mirroring the elevated MAR/PAR signal observed in human I-PE placentas and the LPS-induced rodent model.[120] Upon further analysis, the nitrocellulose membrane probed with an anti-MAR-PAR antibody revealed a prominent band at approximately 120-130 kDa. This band showed a marked reduction in intensity when cells were co-treated with Olaparib during TNF-α stimulation **(Figure 7A)**. Given the expected molecular weight and PARylation profile, this band was hypothesized to correspond to auto-PARylated PARP-1. PARP-1. PARP-1 is known to undergo auto-modification in response to DNA damage and inflammatory

stress, consistent with the observed size shift, as the addition of ADP-ribose chains increases its apparent molecular weight.

To validate this, the nitrocellulose membrane was stripped and re-probe with an anti-PARP-1 antibody, which detected a signal at the same molecular weight, supporting the identification of the band as PARP-1 **(Figure 7C)**. Further analysis of the excised band by liquid chromatography-mass spectrometry (LC-MS) confirmed the presence of PARP-1 among 267 identified proteins. Although multiple proteins were detected, the correspondence in molecular weight and antibody reactivity strongly support our interpretation that this signal represents auto-PARylation of PARP-1. Quantification of this band intensity revealed a significant reduction in MAR/PARylation following Olaparib treatment, confirming effective inhibition of PARP-1/2 under inflammatory conditions **(Figure 7A).** In contrast, XAV939 treatment produced a downward trend that did not reach statistical significance **(Figure 7B)**.

When assessing global protein MAR/PAR levels, normalized to total protein content, co-treatment with TNF-α and Olaparib produced a downward trend compared to TNF-α alone, although not statistically significant **(Figure 7A)**. A similar downward trend was observed with TNF-α and XAV939 co-treatment, though inhibition of TNKS-1/2 produced a smaller reduction in total MAR/PARylation compared with PARP-1/2 inhibition **(Figure 7A)**. These findings indicate that TNF-α – driven MAR/PARylation is predominantly mediated by PARP-1/2 activity, and that Olaparib may be capable of somewhat suppressing this post-translational modification under inflammatory conditions. At 24 hours of treatment, levels of PARP-1 expression were increased with TNF-α and Olaparib co-treatments, along with Olaparib alone. However, PARP-1 expression in trophoblast cells treated with TNF-α showed no changes compared to the vehicle control

(Figure 7D). This may suggest that the increase in MAR/PARylation is due to the increase in enzymatic activity rather than an upregulation in expression.

4.4 Early timepoints show an Increase in PARP-1 MAR/PARylation under TNF-α Inflammatory Conditions.

Upon an inflammatory response, the transition from this response to the activation of PARPs is rapid and can occur within minutes. To examine how early this overactivation of PARPs occurs during a TNF-α induced inflammatory response, levels of MAR/PAR modification were assessed at 30 minutes **(Figure 7E)**. When HTR-8/SVneo trophoblasts cells were treated with TNF-α, MAR/PAR levels trended upwards just after 30 minutes compared to the vehicle control **(Figure 7E)**.

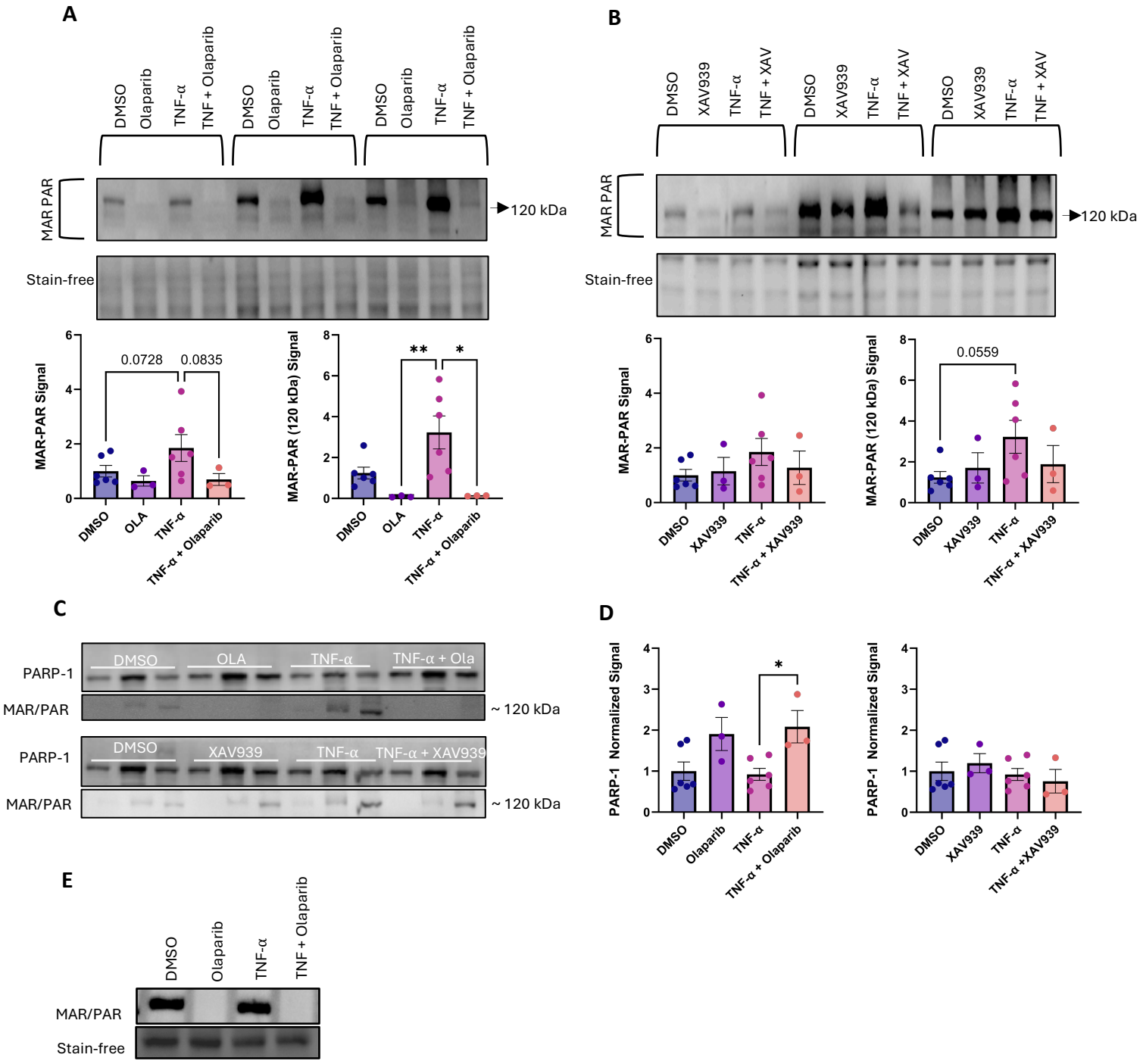

Figure 7. PARP-1/2 Inhibition Reduced MAR/PARylation Protein Modifications under TNF-α-induced Inflammatory Conditions in HTR-8/SVneo cells. HTR-8/SVneo trophoblast cells were treated with TNF-α (10 ng/mL) to induce inflammatory signalling, with or without co-treatments using the PARP-1/2 inhibitor Olaparib (3 µM) or the TKNS-1/2 inhibitor XAV939 (10 µM). MAR/PAR modifications were quantified by western blot to assess the impact of PARP inhibition on TNF-α-induced MAR/PARylation. **(A)** Western blot representing global MAR/PARylation with Olaparib treatment (top) normalized to total protein (bottom) western blot. Densitometry bar graph

showing global MAR/PARylation normalized to total protein (left) and 120 kDa MAR/PARylation normalized to total protein (right). Co-treatment with TNF-α and Olaparib produced a downward trend in global MAR/PAR levels compared to TNF-α alone (left), that became highly significant when specifically examining 120 kDA band (right). **(B)** Western blot representing global MAR/PARylation with XAV939 treatment (top) normalized to total protein (bottom) western blot. Densitometry bar graph showing global MAR/PARylation normalized to total protein (left) and 120 kDa MAR/PARylation normalized to total protein (right). In contrast to Olaparib, co-treatment with TNF-α and XAV939 did not significantly alter total (left) or 120 kDa specific MAR/PAR signal intensity compared to TNF-α alone (right). **(C)** Representative western blots re-probed specifically for PARP-1 after MAR/PAR, confirming the ~120 kDa band corresponds to PARP-1 and showing reduced MAR/PAR signal intensity following PARP inhibition. **(D)** Densitometric quantification of PARP-1 protein expression in Olaparib (left) and XAV939 (right) co-treatments with TNF-α. **(E)** Western blot displays MAR/PAR intensity after 30 minutes of each treatment, showing inhibition of Olaparib and upwards trend in MAR/PAR with TNF-α alone. Statistical significance was determined by one-way ANOVA with Tukey's post hoc test (*p<0.05, ** p<0.01, ***p<0.001). Data are shown as mean ± S.E.M., with individual points representing biological replicates.

4.5 TNF-α-induced inflammation impairs mitochondrial respiration, which is rescued by PARP-1/2 inhibition.

Excessive activation of PARP-1/2 can deplete intracellular NAD^+ stores that are shared with sirtuins (SIRTs), compromising mitochondrial homeostasis and energy metabolism. Because NAD^+ availability supports SIRT-dependent antioxidant and metabolic functions, its depletion during inflammation is expected to impair mitochondrial health. To test whether inhibition of PARP-1/2 could mitigate TNF-α induced mitochondrial dysregulation, mitochondrial respiration was assessed in HTR-8/SVneo EVTs cells using the Seahorse XF Mito-Stress Test following 24 hours of treatment with TNF-α, PARP-1/2 (Olaparib) or TNKS-1/2 (XAV939) inhibitors, alone or in combination.

Basal mitochondrial oxygen consumption rate (OCR), which reflects total mitochondrial oxygen consumption under normal energetic demand, was significantly reduced by TNF-α treatment, indicating a indicating a global suppression of oxidative metabolism **(Figure 8A)**. ATP-linked OCR,

representing oxygen consumption used for ATP synthesis via oxidative phosphorylation, was similarly decreased, confirming reduced mitochondrial ATP production (**Figure 8B**). Proton leak OCR - oxygen consumption not coupled to ATP synthesis and reflective of membrane potential integrity - was also diminished, suggesting decreased mitochondrial membrane efficiency or reduced uncoupling (**Figure 8C**).

Maximal OCR, which indicates the highest respiratory capacity of the electron transport chain (ETC) upon FCCP-induced uncoupling, was markedly attenuated in TNF-α–treated cells (**Figure 8D**). Non-mitochondrial OCR, reflecting oxygen consumption by oxidases or other non-ETC enzymes, trended downward but did not reach statistical significance (**Figure 8E**). The spare respiratory capacity, calculated as the difference between maximal and basal OCR and representing the cell's ability to respond to increased energetic demand, was likewise decreased (**Figure 8F**). Coupling efficiency—the proportion of basal OCR devoted to ATP synthesis versus proton leak—showed little to no change with TNF-α, indicating that the relative partitioning of basal respiration remained largely stable under these conditions (**Figure 8G**).

Treatment with Olaparib or XAV939 alone did not significantly alter OCR parameters under basal conditions. However, co-treatment with TNF-α and Olaparib significantly improved mitochondrial respiration, restoring basal and ATP-linked OCR, as well as spare respiratory capacity and non-mitochondrial OCR **(Figure 8A-G)**. These findings suggest that inhibiting PARP-1/2 activity protects against TNF-α–induced mitochondrial dysfunction, likely through preservation of NAD^+ availability and SIRT activity. In contrast, TNKS-1/2 inhibition with XAV939 failed to rescue TNF-α–induced reductions across most OCR parameters, producing only minor, non-significant improvements **(Figure 8A-G)**. Combined inhibition of PARP-1/2 and TNKS-1/2 modestly elevated

basal OCR and proton leak, further support the conclusion PARP-1/2 activity is the primary driver of inflammation-associated mitochondrial dysfunction in trophoblast cells **(Figure 8A, C)**.

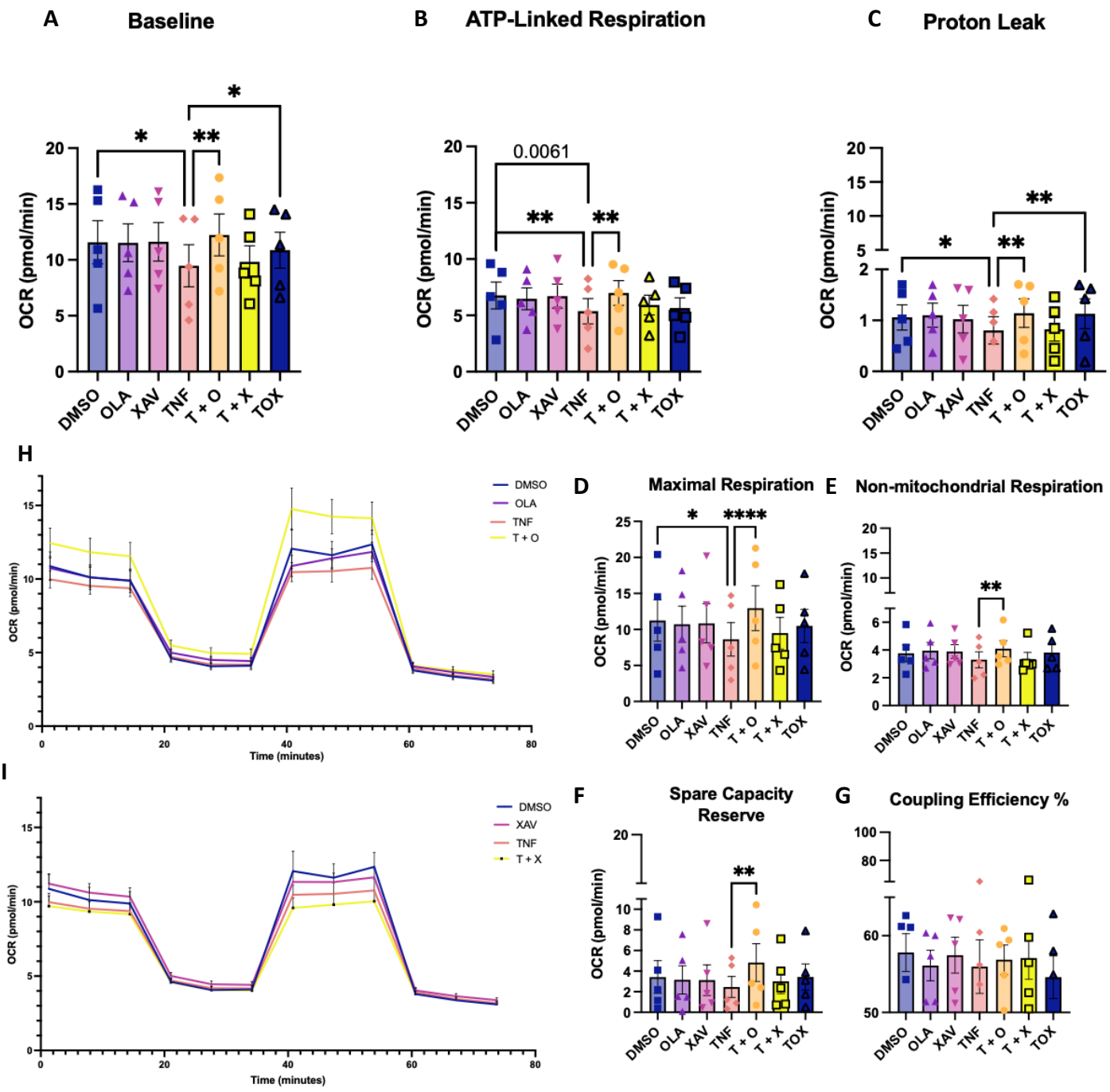

Figure 8. Mitochondrial Respiration in HTR-8/SVneo Cells following TNF-α–induced inflammation and PARP inhibition. Mitochondrial oxygen consumption rate (OCR) was measured in HTR-8/SVneo cells using the Seahorse XF Mito-Stress Test following 24 hours of treatment with TNF-α (10 ng/mL), alone or in combination the PARP-1/2 inhibitor Olaparib (3 µM) or the TNKS-

1/2 inhibitor XAV939 (10 µM). Sequential injections of Oligomycin (1.5 uM), FCCP (1 uM) and Rotenone/Antimycin A (1 uM) were used to interrograte mitchondrial repiratory parameters over a 74-minute assay period, with OCR recorded every 6 minutes. These included: **(A)** Basal respiration - total mitochondrial OCR under resting conditions; **(B)** ATP-linked Respiration - OCR coupled to ATP synthesis via oxidative phosphorylation; **(C)** Proton leak - OCR not used for ATP synthesis, indicative of mitochondrial membrane integrity; **(D)** Maximal Repiration - OCR following FCCP uncoupling, representing the ETC's full capacity; **(E)** Non-mitochondrial Respiration - OCR from non-ETC sources such as oxidases; **(F)** Spare Capaicity Reserve - the difference between maximal and basal OCR, indicating the ability to respond to energetic stress; **(G)** Coupling Efficiency - the proportion of basal OCR used for ATP production versus proton leak. Representative kinetic OCR traces showing temporal respiration profiles for TNF-α with co-treatments of **(H)** Olaparib and **(I)** XAV939. Data are presented as mean ± S.E.M. (n = 5 biological replicates). Statistical significance was determined by one-way ANOVA with Tukey's post hoc test (*p<0.05, ** p<0.01, ***p<0.001).

4.6 No alterations in OXPHOS protein expression during TNF-α-induced Inflammation.

TNF-α is well known to induce oxidative stress, lipid peroxidization and mitochondrial dysfunction across multiple cell types. In HTR-8/SVneo trophoblast cells, we previously demonstrated tat TNF-α treatment increased MAR/PARylation and disrupts mitochondrial respiration, consistent with our proposed mechanism of PARP overactivation and NAD^+ depletion. To determine if the observed mitochondrial dysfunction resulted from altered expression of OXPHOS complexes, we next quantified the protein levels of individual electron transport chain (ETC) components (Complexes I–V). Western blot analysis revealed no changes in the expression of any OXPHOS complexes following TNF-α treatment, either alone or in combination with PARP inhibition **(Figure 9 A-K)**. These results indicate that the impaired mitochondrial respiration observed under inflammatory conditions is not due to decreased abundance of OXPHOS proteins. Instead, the data suggest that post-transitional mechanisms, such as PARylation-mediated modulation of enzyme activity or disruptions in NAD^+-dependent signaling, are responsible for the observed reductions in mitochondrial function.

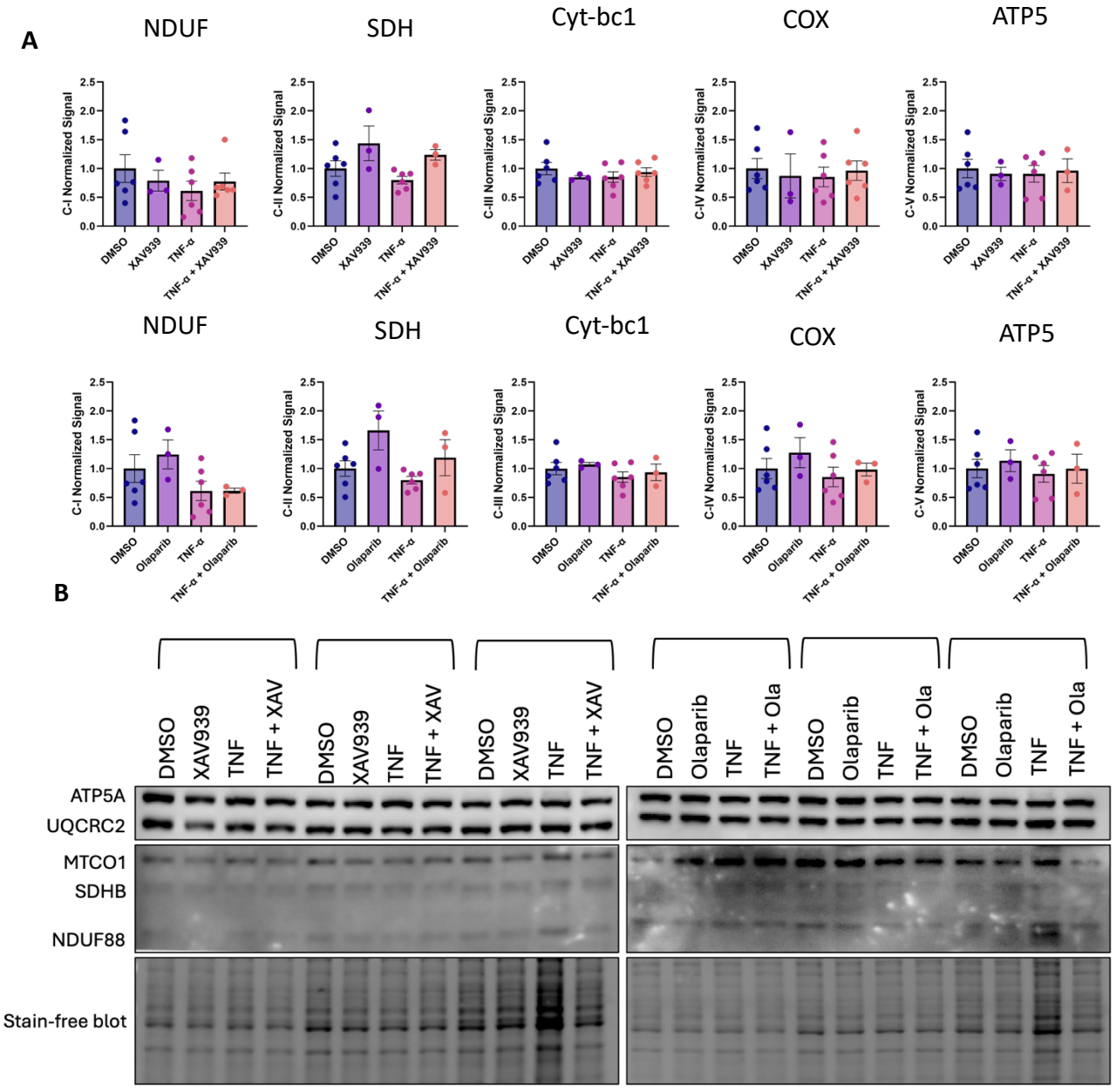

Figure 9. Expression of OXPHOS Complex Proteins in HTR-8 Cells Following PARP Inhibition under Inflammatory conditions. HTR-8/SVneo cells were treated with TNF-α (10 ng/mL) to induce an inflammatory response, with or without co-treatment of the PARP-1/2 inhibitor Olaparib (3 µM) or the TNKS-1/2 inhibitor XAV939 (10 µM). After 24 hours, protein was extracted and analyzed by Western blot for the expression of oxidative phosphorylation (OXPHOS) complex subunits. Densitometric quantification of OXPHOS components is shown for **(A)** C-I NDUF, C-II SDH, C-III Cyt-bc1, C-IV COX C-V ATP5 for Olaparib co-treatments, and corresponding complexes for XAV939 co-treatments. **(B)** Representative Western blot images for each treatment group are

shown. Data are presented as mean ± S.E.M (n=3 biological replicates). Statistical significance was determined using a one-way ANOVA and Tukey's post hoc test (*$p \leq 0.05$).

4.7 TNF-α - Induced Inflammation does not alter Lipid Peroxidation.

Lipid peroxidation is a hallmark of oxidative stress resulting from the reaction of highly reactive oxygen species (ROS) with polyunsaturated fatty acids (PUFAs) in serves as a widely recognized biomarker for oxidative damage in various disease contexts. TNF-α is also known to promote oxidative stress through activation of pro-inflammatory signalling pathways, including those involving NF-kB and NADPH oxidases.

In our proposed mechanism, excessive PARP activation depletes intracellular NAD^+ levels, thereby reducing SIRT activity and weakening the cell's antioxidant defenses. To determine whether PARP-1/2 inhibition could mitigate oxidative stress downstream of TNF-α signalling, we quantified 4-HNE levels in HTR-8/SVneo EVTs by Western Blot following 24 hours of treatment with TNF-α, with or without PARP inhibition.

Across all treatment groups, no statistically significant differences in 4-HNE levels were observed ($p > 0.05$; **Figure 10A-B)**. The absence of detectable changes suggests that TNF-α–induced oxidative stress at this time point does not manifest as increased lipid peroxidation in HTR-8/SVneo cells. Alternatively, lipid peroxidation may occur earlier in the inflammatory response or may not be a dominant oxidative stress pathway in this trophoblast model.

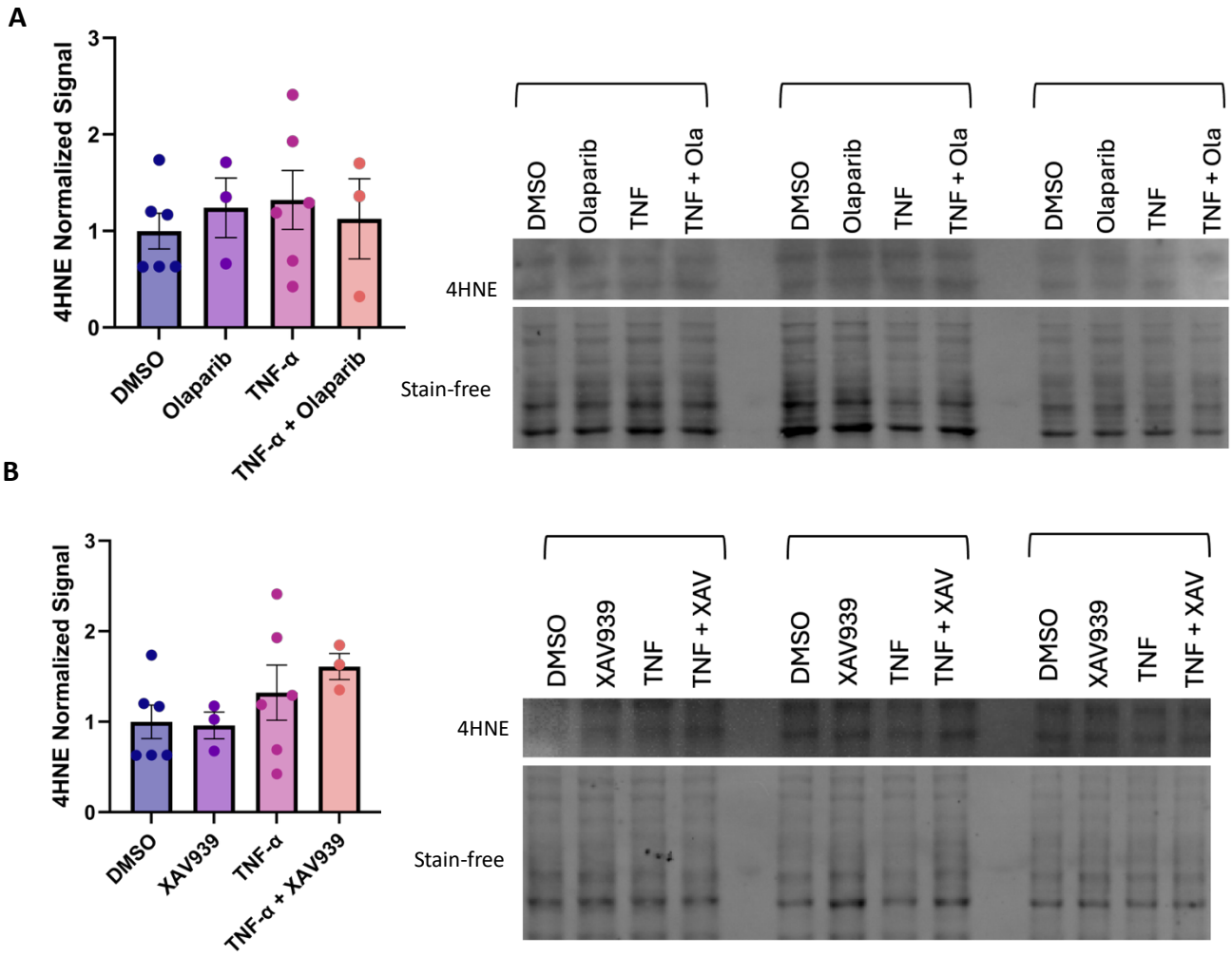

Figure 10. Expression of 4-HNE as a marker of lipid peroxidation and oxidative stress in HTR-8/SVneo Cells during Inflammatory Insult. HTR-8/SVneo cells were treated with TNF-α (10 ng/mL) to induce an inflammatory response, with and without co-treatments with the PARP-1/2 inhibitor Olaparib (3 µM) or the TNKS-1/2 inhibitor XAV939 (10 µM). DMSO served as a vehicle control. After 24 hours of treatment, total protein extracts were collected, and to 4-Hydroxynonenal (4-HNE) levels were quantified by Western blot as an indicator of lipid peroxidation. **(A)** Densitometric quantification of 4-HNE signal intensity was normalized to stain-free total protein blots. **(B)** Representative western blot images of 4-HNE signal and corresponding stain-free blots are shown. Data are presented as mean ± S.E.M (n = 3 biological replicates).

4.8 Olaparib restores trophoblast migration supressed by TNF-α-induced inflammation.

Having established that TNF-α impairs mitochondrial respiration in HTR-8/SVneo trophoblasts and that this deficit can be rescued by PARP-1/2 inhibition, we next examined whether these metabolic alterations translated into functional consequences. Extravillous trophoblast cells (EVTs) play a crucial role in migrating and invading into the maternal endometrium to establish the utero-placenta interface and remodel spiral arteries into blood supply to the developing fetus. EVTs play an important role anchoring the chorionic villi to the decidua, providing a secure connection between the mother and the fetus. In addition, EVTs are responsible for vascular remodelling of maternal spiral arteries, replacing endothelial tissues with smooth muscle tissues – creating low-resistance spiral arteries. HTR-8/SVneo cells are widely used to assess the migration and invasive function of EVTs in preeclampsia, amongst other diseases. Here, we sought out to investigate if TNF-α induced inflammation affected the migrating function of trophoblast cells through PARP-1/2 overactivation. Scratch wound assay was used to assess the migration function of HTR-8/SVneo, simply by creating a scratch on the plate and comparing the wound area after 24 hours. Differences in wound confluence % did not reach statistical significance, however trends across experimental treatments support our hypothesis in our proposed mechanism. The wound confluence % of HTR-8/SVneo cells exposed to a TNF-α induced inflammation, was trending downwards compared to the vehicle control **(Figure 11A-B)**. During this TNF-α inflammatory insult, EVT migration may be restored with PARP-1/2 inhibition by

Olaparib as the wound confluence % trended upwards, improving migration function. Inhibition of TNKS-1/2 combined with TNF-α inflammation was not able to restore EVT migration function **(Figure 11A-B)**. These trends support our hypothesis in that – the overactivation of specifically PARP-1/2, suppresses the function of EVT in migrating downstream of I-PE mechanism.

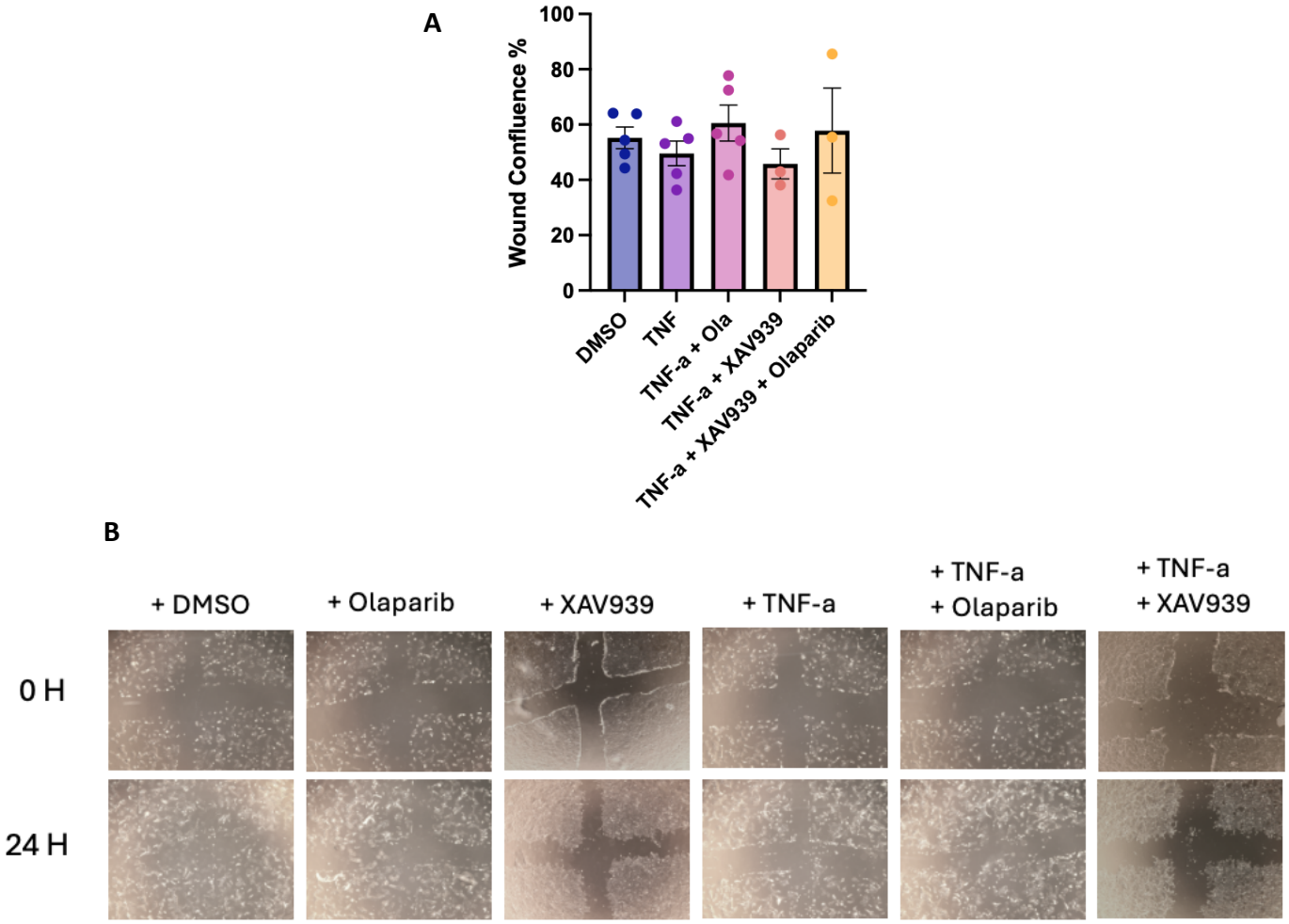

Figure 11. Trophoblast Migration Function Assessed by Scratch Assay Following PARP Inhibition during Inflammatory Insult. The migration function of HTR-8/SVneo was assessed using the scratch migration assay by allowing the cells to grow to 90-100% confluency followed by a 6H starvation period. Each well was scratched vertically and horizontally and treated with different experiments including TNF-α (100 ng/µL) to stimulate an inflammatory response along with separate co-treatments of Olaparib (3 µM) and XAV939 (10 µM). DMSO was used as a vehicle control. After 24 hours of treatment, final images were captured using Invitrogen™ EVOS™ XL

Core [Imaging System (Fisher Scientific) at 10X. Scratch area was quantified, and the wound confluence percentage area was calculated as described by Ranzoni et al.[160] **(A)** Wound confluence quantification data is presented as mean ± S.E.M. Individual data points represent biological replicates (n=5). Statistical significance was determined using a one-way ANOVA and Tukey's post hoc test (*$p < 0.05$). **(B)** Representative images of the intersection of the scratch at 0 hour and 24 hour is shown for each treatment.

4.9 TNF-α alone or combined with PARP-1/2 inhibitors does not show any signs of cytotoxicity

The final step in our proposed mechanism from a TNF-α induced inflammation is the activation of cytotoxicity pathways, leading trophoblast to cell death. TNF-α induced cell death is well-established in pro-inflammatory signalling where TNF-α can induce cytotoxicity by triggering multiple, and in some condition, overlapping apoptotic pathways. Multiple studies have reported cell death as early as 6 hours and as late as 48 hours depending on the cell type or the pathways that are activated. Given that, our previous results showed signs of mitochondria dysfunction and a reduction in migration function at 24 hours, we sought out to confirm if cytotoxicity signs would be detectable at this timepoint. Cell viability was assessed using the Calcein-AM assay that measures the relative fluorescence units (RFU) of live cells. Viable cells can hydrolyze non-fluorescent Calcein-AM into a fluorescent molecule that is directly proportional to cell viability. This assay is widely used across different studies to measure cell viability and membrane integrity. As this is not a measure of cell death, Calcein-AM assay was used to assess the change in viability in trophoblast cells. In contrast to many studies, under our conditions, there are no significant changes in cell viability in between any of the experimental treatments showed at 24 hours **(Figure 12)**. Collectively, these observations can suggest that trophoblast cytotoxicity may be at later timepoint or does not occur in I-PE

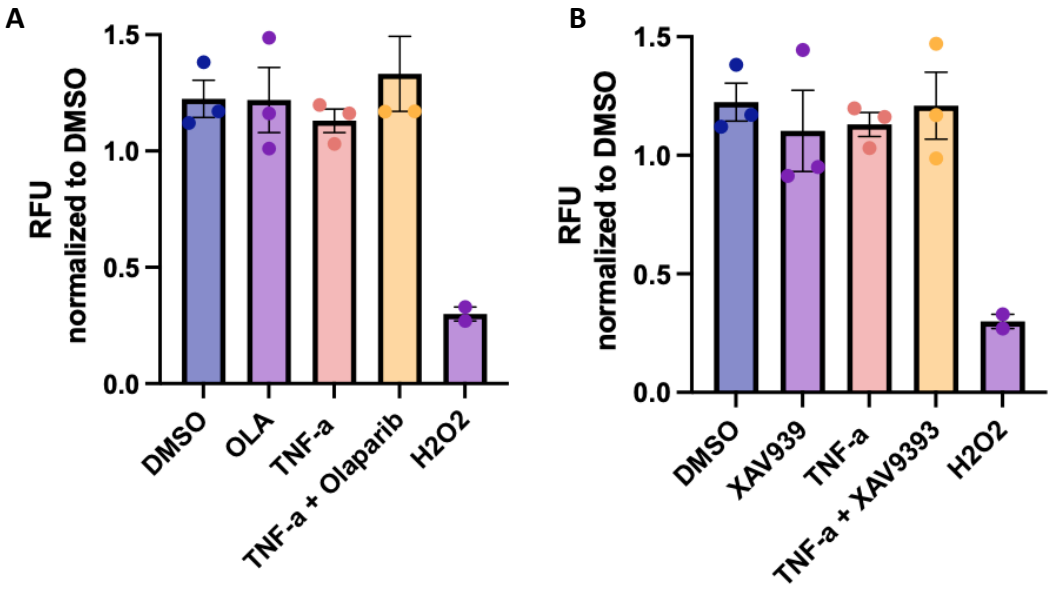

Figure 12. Trophoblast Calcein-AM Viability Following PARP Inhibition Under Inflammatory Conditions. HTR-8/SVneo cells were plated for 24 hours following by a treatment of the different groups. HTR-8/SVneo cells were treated with TNF-α (10 ng/mL) to stimulate an inflammatory response. **(A)** Olaparib (3 µM) and **(B)** XAV939 (10 µM) were added separately to TNF-α as a co-treatment to investigate the effects of PARP activation in cell viability. DMSO served as a vehicle control, H2O2 served as a cytotoxicity control. After 24 hours, cells were washed twice with 1X PBS, before adding Cell Dye II/Calcein AM buffer and reading the fluorescence at Ex/Em = 485/530 nm. Calcein fluorescence was quantified using POLARstar Omega plate reader (BMG Labtech). Data is presented as mean ± S.E.M. Individual data points represent biological replicates (n=3). Statistical significance was determined using a one-way ANOVA and Tukey's post hoc test (*$p < 0.05$).

4.10 PARP-1 linked MAR/PAR modification target associated to Immune response pathways in HTR-8/SVneo cells.

Previously mentioned, PARP-1 confirmation was observed with western blots at the specific region where MAR/PAR modifications were increased with TNF-α and inhibited specifically with PARP-1/2 inhibitor, Olaparib. We questioned ourselves if there were any other target of MAR/PARylation and if there were targets of PARP-1 specifically. Across 267 identified proteins,

203 (76%) were known to be target of MAR/PARylation modifications – of those protein, 143 (70%) were known PARP-1 targets. **(Figure 13A)**. The majority of PARP-1 targets are known to be PARylated rather than MARylated **(Figure 13B)**.

To further examine these proteins, reactome enrichments pathways were performed in the proteins located at this specific molecular weight that are known targets of PARP-1 – to gain insights of what pathways are involved. **(Figure 13C)**. Most prominent enrichment pathway with a high gene count was immunological activated proteins – this includes metabolism of proteins, activated innate immune system and cellular responses to stress. Multiple studies have reported alterations in protein metabolism upon pro-inflammation responses. In our dataset, additional pathways exhibit strong evidence of post-translational protein modifications, cytokine signalling in immune systems and common pathways that link the overactivation of PARP-1/2 and TNF-α induced inflammation **(Figure 13C)**.

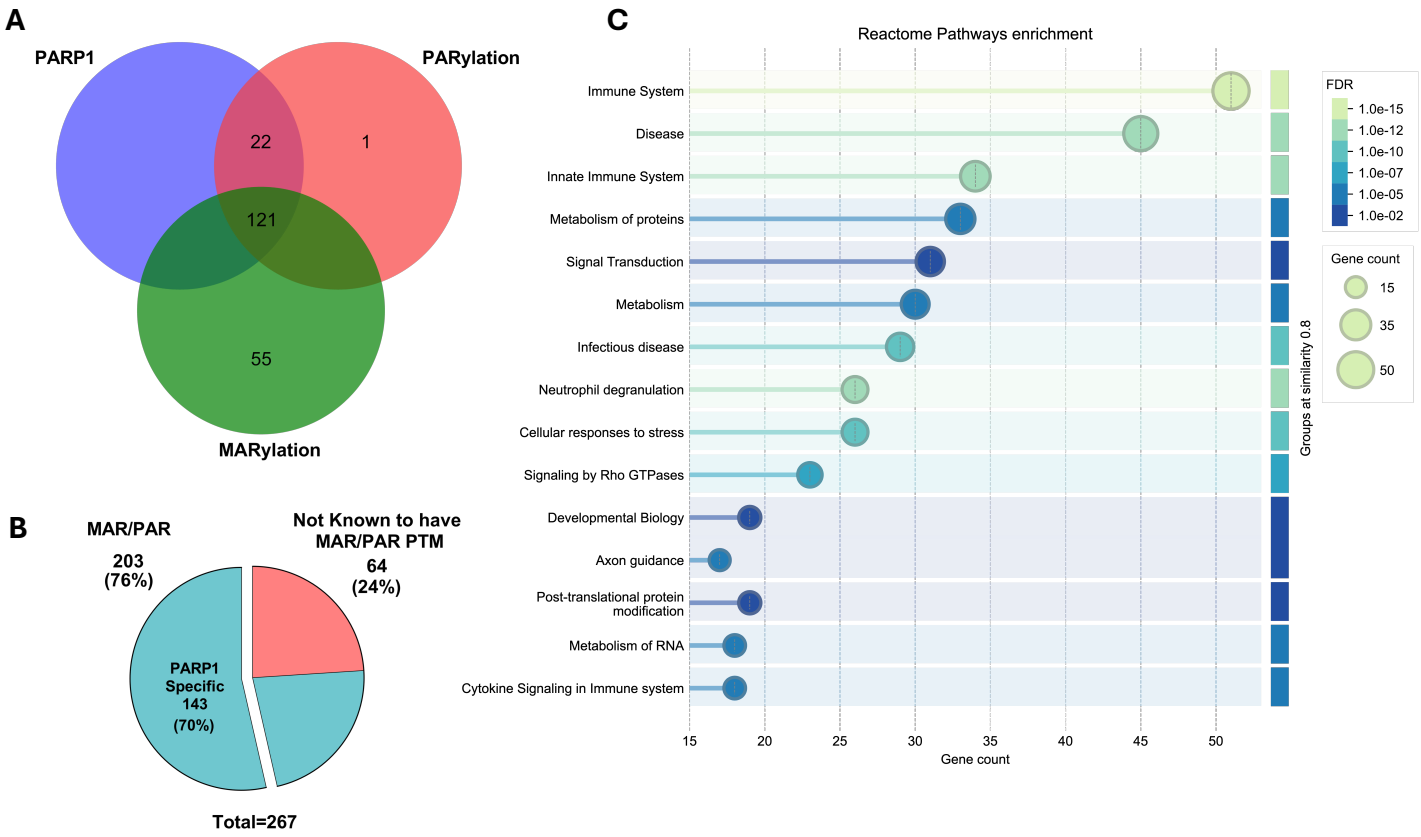

Figure 13. MAR/PAR Modification of Proteins found in MALDI-MS Analysis. Nitrocellulose membranes (Figure. 7 D-E) were cut to separate the region of interest for PARP-1 confirmation at ~ 120 kDa. List of proteins that were found at this molecular weight were analyzed. **(A)** Pie-chart of the full list of proteins found at this region. **(B)** Venn diagram of the proteins demonstrates the shared protein identification of PARylation, MARylation and PARP-1 specific targets. **(C)** Reactome pathway enrichment showing protein-protein interaction network using STRING platform (string-db.org).

5 DISCUSSION

Inflammation-mediated preeclampsia (I-PE) remains to be the subclass of PE that is the least understood in both the molecular mechanism and physiology of this disease. There is compelling evidence that links the instability of NAD^+ metabolism to inflammatory diseases, oxidative stress and mitochondria disease.[120,137,164] Nonetheless, despite their established role in inflammatory diseases, the role of NAD^+ in placenta biology remains largely unidentified. Previously, our group was the first to study the role of NAD+ in placenta health and identified two phenotypes that are unique to I-PE.[120]

1. NAD+ depletion in the intracellular stores of human cases of I-PE
2. Increase in PARylation levels in placenta tissues of I-PE cases

As there are 4 out of the 17 PARPs members that exhibit PARylation activity, the increase in PARylation levels that are causing this rapid depletion on NAD^+ intracellular stores was unknown. In the presence work, I have provided evidence that the increase in PARylation is consequently due to the overactivation of auto-PARylated PARP-1 in HTR-8/SVneo EVT induced with TNF-α Inflammation.

TNF-α is key signalling cytokine that plays an important role in inflammation, obesity, and fighting against infections.[22,44,165] Under prolonged inflammatory responses, extensive research has established that excessive TNF-α accumulation can eventually lead to the development of chronic inflammatory diseases.[166,167] The mechanism behind TNF-α and PARP-1 overactivation has been well-established under pro-inflammation conditions. [168–170] TNF-α acts as a signalling molecule and binds to its receptor - Tumour Necrosis Factor Receptor (TNFR), activating a cascade of kinase events involved with the Mitogen-activated protein kinase (MEK)/ Extracellular-signal-regulated

kinase (ERK) pathways. Eventually, PARP-1 is phosphorylated by ERK-1/2 – leading to the overactivation of PARP-1 PARylation. In addition, PARP-1 can increase its own activity by PARylating itself, which is observed across many molecular processes. To date, this molecular mechanism remains undefined in placenta health and function.

Analysis of mRNA expression of PARPs across the two different models of I-PE show variation in PARP-1 transcription. Outside of the placenta, studies focusing on inflammatory conditions have reported no changes in PARP-1 mRNA or protein expression – thus, suspecting the increasing in PARylation, is a result of increased enzymatic activity. In placenta tissue, the human protein atlas reports that PARP-1 at the mRNA and protein level is highly expressed in cytotrophoblast cells compared to extravillous trophoblast cells. In cytotrophoblast cells, PARP-1 is a key regulator in the differentiation into syncytiotrophoblast cells during placental development (**Figure 14A-B**).

In our study, LPS-induced rodents have trends of PARPs mRNA increases – which could be coming from the lack of sensitivity to this immune response, needing a boost of PARP-1 at the transcription level to increasing PARylation. Recent evidence has reported the increase of PARP-1 expression through the activation of nuclear factor kappa-light-chain-enhancer of activated B cells (NF-κB) pathways under inflammatory conditions. Under prolonged TNF-α conditions, some studies have demonstrated that PARP-1 PARylation of RelA (p65 subunit) is required for NF-κB transcription.[171] RelA (p65 subunit) is a transcription factor of NF-κB, that has shown evidence of promoting the transcription of PARP-1 as well. NF-κB and PARP-1 regulate each other in a positive-feedback loop – amplifying and sustaining this inflammatory response enhancing the production of TNF-α. These mediators of immune-mediated inflammation are driven and positively influence each other creating the pathogenesis of chronic inflammatory disease.[172]

PARP-1 overactivation is associated with intracellular NAD^+ depletion across various inflammatory diseases. NAD^+ is an essential co-factor involved in redox reactions, energy metabolism, cell signalling, and mitochondrial health. Previous members from our group confirmed this NAD^+ depletion across the three models of I-PE. Levels of NAD^+, NADt (NAD^+ and NADH) and NAD^+ /NADH ratios were measured and revealed a decreased in NAD^+ and NADt, however NADH levels remain unchanged. NAD^+ is metabolized in separate cellular sub-compartments including the mitochondria, cytosol and nucleus – each possessing their own pool of NAD^+. The NAD^+ concentrations in each cellular sub-compartment are cell-type dependant as the range of concentrations of NAD^+ can vary as well of the distribution of NAD^+ to each sub-compartment. The NAD^+ concentration in healthy placenta in mice is approximately 0.17 umol/gProt in the mitochondrial, 0.2 umol/gProt in the cytoplasm and 0.015 umol/gProt in the nucleus.[173] The concentration distribution of NAD^+ has not even investigated n HTR-8/SVneo cell model. Nuclear NAD^+ pools are mainly used by NAD^+ heavy consuming enzymes such as PARPs and SIRTs, generating NAM as a by-product. In the mitochondria, NAD^+ is reduced into NADH in the TCA cycle for the purpose of energy production during oxidative respiration. Studies have observed an increased in NAM levels, yet NADH levels are not affected during PARP-1 overactivation, suggesting that nuclear NAD^+ pools are not directly affecting the mitochondrial NAD^+ stores.[120] The mechanism by which the sub-compartments of NAD^+ pools have not affected by each other is unknown.

Nonetheless, PARP-1 overactivation is associated with mitochondrial dysfunction downstream of its mechanism. As previously mentioned, nuclear NAD^+ pools are mainly shared between PARPs and SIRTs. Under pro-inflammatory conditions, PARPs and SIRTs have an antagonistic relationship

and compete for NAD^+ stores, often leading to rapid depletion of NAD^+ used by PARP-1 and comprising the activity of SIRTs. During the activation of PARP-1 PARylation, studies have reported that a depletion of 80% of NAD^+ levels compared to total intracellular NAD^+. [174,175] SIRTs play an essential role during PARP-1 overactivation by promoting anti-inflammatory cytokines and suppressing the production of pro-inflammatory cytokines. Not only does it have a protective role in mitochondrial health, but it also essential in placenta development and differentiation. Our LPS-induced rodent model shows an increase in the transcription of SIRTs that suggest it may be recompensating for the reduction in activity. The Human Protein Atlas indicates that SIRTs expression in placenta tissue is generally highly expressed compared other tissue types, suggesting it's important role in placenta health and function (for example SIRT4; **Figure 14C**). As previously mentioned, NF-κB and PARP-1 overactivation in inflammatory diseases drive the activation of both pathways. SIRT-1 activity inhibits the activation of NF-κB pathways by deacetylating the p65 subunit – transcription factor of NF-κB and decreasing pro-inflammatory cytokine production. PARP-1 overactivation inhibits SIRT activity in protecting against NF-κB pathways, further exacerbating the inflammatory response.

The imbalance in inflammatory cytokines generally leads to the production of oxidative stress and the increase in ROS production. ROS levels could increase through the TNF-α-signalling pathways or through mitochondrial dysfunction. 4-HNE is common marker in lipid peroxidation and oxidative stress, observed during PARP-1 activation. In TNF-α treated HTR-8/SVneo cells, there were no significant changes in 4-HNE levels at 24 hours. Multiple studies have reported rapid changes in 4-HNE, with detectable changes at earlier timepoints within the first hour to 24 hours depending on the cell line and stimulation.[176,177] In colorectal cancer cells, TNKS-1/2 has been

linked to the inactivation of oxidative stress - suggesting that inhibiting TNKS-1/2 may eliminate its protective role against cellular stress, however this mechanism is not fully understood.[178] Compelling evidence indicates, an accumulation of 4-HNE can directly and indirectly impair mitochondrial health by altering the structure/function of OXPHOS complexes and further activating cellular stress pathways.[179]

Mitochondrial dysfunction is a hallmark of preeclampsia, commonly seen across all subclasses of PE. As we've seen previously, nuclear SIRTs activity is inhibited during the overactivation of PARP-1, that directly affects the expression and activity of mitochondrial SIRTs. Here, we've reported that PARP-1/2 inhibition rescues mitochondrial health and function during a TNF-α-induced inflammation in trophoblast cells. PARP-1/2 overactivation reduces baseline levels, ATP-linked-respiration, maximal respiration, proton leak, spare capacity reserves and non-mitochondrial respiration. This suggest that instead of PARP-1 affecting specific complexes, it is impairing the overall health of the mitochondria. During inflammatory responses, studies have generally observed increases in non-mitochondrial respiration from cytosolic oxidases.[180] In contrary, under our condition we have reported a decrease in non-mitochondrial oxygen consumption - in which the mechanism behind this remain unknown. The decrease in oxidative respiration may also be comprised by mitochondrial biogenesis repressors. SIRT-1 is responsible for the deacetylation of PCG-1α – master transcription factor of mitochondria biogenesis and function. PARP-1 overactivation can lead to SIRT-1 inhibition, reducing mitochondria mass and integrity. The expression of OXPHOS protein did not change under TNF-α conditions, however trends reveal slight increases with PARP-1/2 inhibition – aligning with other studies. In addition, our previous study, reveals that the population of the I-PE subclass show an increased trend in maternal age

compared to other subclasses of PE.[35] The prevalence of preeclampsia increases in mother from age 35-40 and doubles after 40 years compared to the general population of pregnant women.[181] This supports our hypothesis that a decline in mitochondrial function is a hallmark of aging.

Migration and invasive capacity are the primary functions of extravillous trophoblast cells in establishing a strong utero-placental circulation by migrating and invading into the decidua. Mitochondrial dysfunction has previously been linked to reduced trophoblast function; however, the exact mechanism is not known. ATP depletions from mitochondrial dysfunction have been associated to the inhibition of invasive capacity and migration.[182] This ATP depletion can be produced from the impairment of oxidative respiration processes in the production of ATP. Alternatively, ATP can also be depletion for its usage in the salvage pathways, producing NAD^+ from its by-product NAM in PARylation. Here, I have demonstrated that PARP-1/2 inhibition may restore migrating function of EVTs that may be inhibited by TNF-α inflammatory activation. TNKS-1/2 inhibition was not able to restore migration capabilities with TNF-α treated EVTs, aligning with our hypothesis that PARP-1 PARylation may be responsible for inhibiting migration in EVTs.

Inflammatory pathways, mitochondrial dysfunction pathways and the accumulation of oxidative stressors are all common phenotypes that have strong evidence of eventually leading to cell death. Under different conditions, PARP-1 has the ability to promote or suppress cell death depending on the activated pathways. The canonical pathway of PARP-1 is involved with DNA damage repair, recruiting DNA repair proteins and altering chromatin structures to facilitate with DNA repair. In the case where DNA damage is far beyond repair and there is an accumulation of nuclear PAR, PARP-1 is able to activate regulated apoptotic pathways. In addition, excessive activation of PARP-1 under inflammatory reactions can trigger necrosis, a form of cell death under

cellular stress. Energy exhaustion or ATP depletions from the increase in PARylation is a major contribution to necrosis under PARP-1 activation. Furthermore, the rupture of necrotic cells further activates inflammatory responses to surrounding cells, amplifying this response. In our study, TNF-α induced inflammation did not affect cell viability in EVTs at 24 hours. In trophoblasts, differences may become detectable at later timepoints with a prolonged exposure of TNF-α.

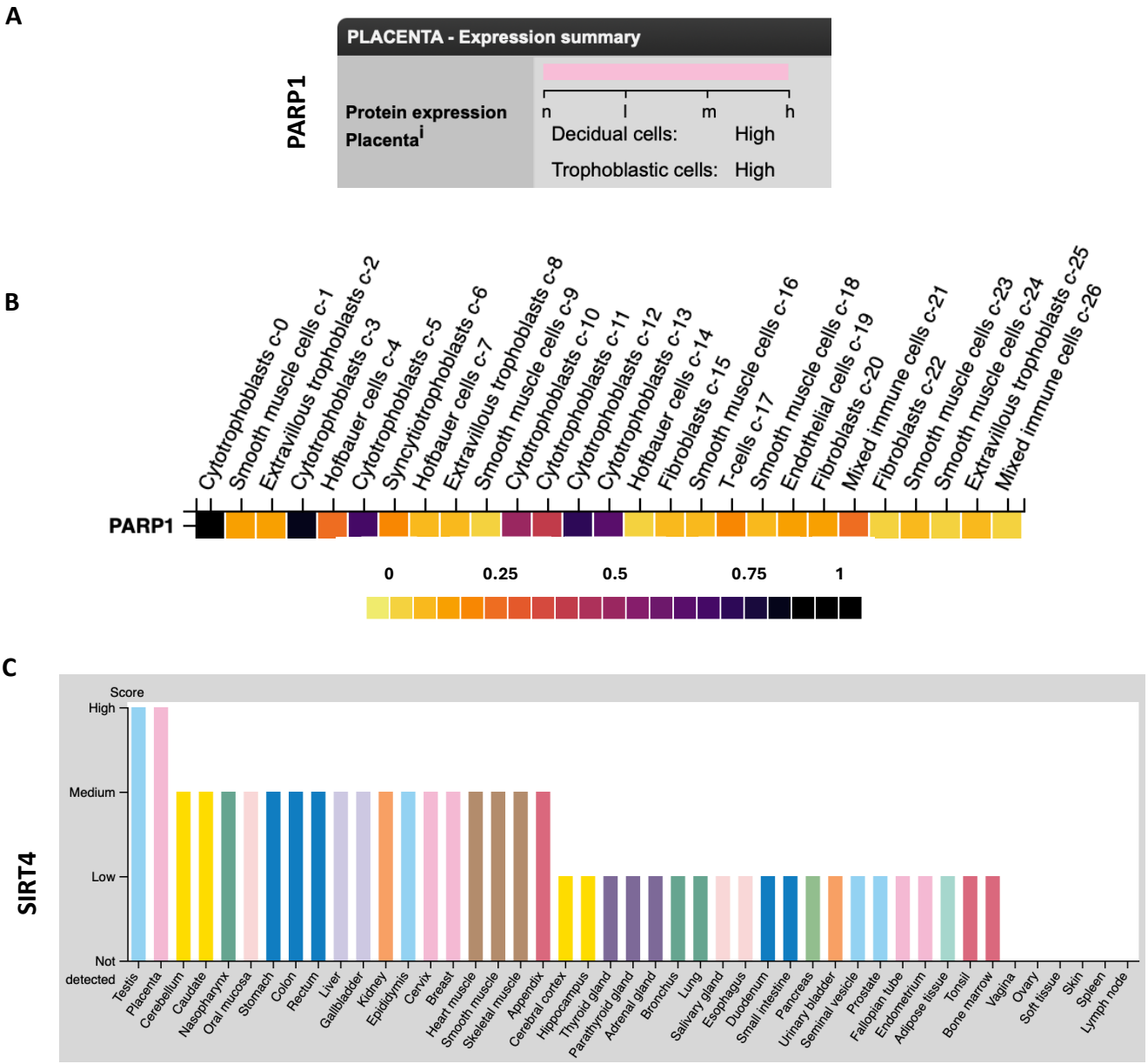

Figure 14. Human Protein Atlas: Expression of NAD+ Consumers in Placenta Tissue. PARP-1 **(A)** protein expression and **(B)** mRNA expression in placenta tissue and cells. Abbreviation n: Not detected, l: Low expression, m: medium expression and h: High expression. **(C)** mRNA expression of SIRTs across different organs, revealing a high score in placenta tissue. Images were obtained from the Human Protein Atlas.

6 Limitations

The findings of this project gave us insights on the effects of PARP-1/2 inhibition on TNF-α-induced inflammation in extravillous trophoblast cell model. One of the primary limitations of this study lies on the HTR-8/SVneo trophoblast in-vitro model that is used to mirror the effect of I-PE in pregnant populations. The human immune system is extremely complex, diverse and dynamic, that 2D in-vitro models cannot fully reproduce the responses we see in humans. I-PE is immune-mediated disease in humans that is activated by an initiated immune response. During early pregnancy, the population of immune cells could reach to 70% in the placenta and is reduced to ~40% after the first trimester until delivery. Immunological analysis of I-PE placenta exhibits an increased in filtration of adaptive and innate immune cells that are absent in-vitro. In HTR-8/SVneo model, the lack of immune cells limits this project as it does not allow us to observe the effects of the surrounding environment during this response as we have seen in the human placenta.

Furthermore, we are using a TNF-α recombinant protein to initiate this immune response from HTR-8/SVneo EVTs as we see in I-PE. As previously mentioned, TNF-α is the central role in activating an immune response in I-PE. Nonetheless, a multi-omics analysis of I-PE has confirmed various upregulations of pro-inflammatory cytokines and downregulations of anti-inflammatory cytokines that lead to the activation of multiple immunology pathways.

Another limitation in this study is the RNA quality that may affect the results of the gene expression in human placenta samples. Acquiring a high yield of RNA with high Integrity and quality is quite difficult in human placenta collection. There are two main factors during the delivery of the placenta that is essential to the RNA integrity that affects the quality of our data.

The first factor is timing, where it is unknown how long the placenta was at room temperature before taking a tissue sample and freezing it. The second factor is how the tissue was stored before RNA extraction. Placenta tissue that was handled and dissected before storage generally exhibit a low RNA integration number (RIN) than tissues that were immediately stored flash frozen (FF) or using an RNA-stabilizing solution (RNALater).[183] The samples used in the mRNA analysis were purchased from the Research Centre for Women's and Infants' Health BioBank (RCWIH), with no knowledge of how these samples were collected.

7 Conclusion

In this thesis, I have provided insights on the mechanism behind I-PE and how the activated immune response is affecting the overall health of extravillous trophoblast. Previously, the PARP member that is responsible for excessive PARylation activity and a rapid NAD^+ depletion was not well-defined in I-PE. In HTR-8/SVneo cells treated with an TNF-α inflammatory insult reduced the oxygen consumption in multiple mitochondrial parameters and increased lipid peroxidation levels thus damaging the mitochondrial health and function. In addition, visible trends show the inhibition of the migrating function and a reduction in viability in trophoblast cells treated with TNF-α. EVT cells co-treated with only PARP-1/2 inhibitor and TNF-α rescued the effect of its pro-inflammatory insults, however these results were not reproduced with TNKS-1/2 inhibitor. Here we have confirmed that PARP-1 is the member of the PARP family that is mainly responsible for this increase in PARylation causing the depletion in intracellular NAD^+ levels. The findings from this study help elucidate the development of immune-mediated preeclampsia and define the underlying mechanisms that may aid in identifying targets to prevent or attenuate I-PE, while also supporting our hypothesis regarding NAD^+ supplementation during pregnancy. PARP1/2

inhibition in this study shows improved cellular function and health, however it should be noted that PARP1/2 inhibition is not recommended during pregnancy as it can cause serious harm in the development of the fetus.

References

1. Say, L. *et al.* Global causes of maternal death: a WHO systematic analysis. *Lancet Glob. Health* **2**, e323–e333 (2014).

2. Turbeville, H. R. & Sasser, J. M. Preeclampsia beyond pregnancy: long-term consequences for mother and child. *Am. J. Physiol. - Ren. Physiol.* **318**, F1315–F1326 (2020).

3. Alonso-Ventura, V. & Pérez-López, F. R. Preeclampsia negatively affects future maternal metabolic and endocrine outcomes. *Gynecol. Endocrinol.* **37**, 773–774 (2021).

4. Hammoud, G. M. & Ibdah, J. A. Preeclampsia-induced Liver Dysfunction, HELLP syndrome, and acute fatty liver of pregnancy. *Clin. Liver Dis.* **4**, 69–73 (2014).

5. Than, N. G. *et al.* Early pathways, biomarkers, and four distinct molecular subclasses of preeclampsia: the intersection of clinical, pathological, and high-dimensional biology studies. *Placenta* **125**, 10–19 (2022).

6. Roberts, J. M. & Hubel, C. A. The Two Stage Model of Preeclampsia: Variations on the Theme. *Placenta* **30**, 32–37 (2009).

7. Macedo, T. C. C. *et al.* Prevalence of preeclampsia and eclampsia in adolescent pregnancy: A systematic review and meta-analysis of 291,247 adolescents worldwide since 1969. *Eur. J. Obstet. Gynecol. Reprod. Biol.* **248**, 177–186 (2020).

8. Koulouraki, S. *et al.* Short- and Long-Term Outcomes of Preeclampsia in Offspring: Review of the Literature. *Children* **10**, 826 (2023).

9. Preeclampsia | Hypertension. https://www.ahajournals.org/doi/10.1161/01.HYP.0000188408.49896.c5.

10. Establishment of the Human Uteroplacental Circulation: A Historical Perspective - PubMed. https://pubmed.ncbi.nlm.nih.gov/27733657/.

11. Wang, Y. & Zhao, S. Placental Blood Circulation. in *Vascular Biology of the Placenta* (Morgan & Claypool Life Sciences, 2010).

12. The trophoblast plug during early pregnancy: a deeper insight | Histochemistry and Cell Biology. https://link.springer.com/article/10.1007/s00418-016-1474-z#.

13. Sparks, J. W., Hay, W. W., Meschia, G. & Battaglia, F. C. Partition of maternal nutrients to the placenta and fetus in the sheep. *Eur. J. Obstet. Gynecol. Reprod. Biol.* **14**, 331–340 (1983).

14. Gude, N. M., Roberts, C. T., Kalionis, B. & King, R. G. Growth and function of the normal human placenta. *Thromb. Res.* **114**, 397–407 (2004).

15. Brett, K. E., Ferraro, Z. M., Yockell-Lelievre, J., Gruslin, A. & Adamo, K. B. Maternal–Fetal Nutrient Transport in Pregnancy Pathologies: The Role of the Placenta. *Int. J. Mol. Sci.* **15**, 16153–16185 (2014).

16. Salomon, C., Yee, S. W., Mitchell, M. D. & Rice, G. E. The Possible Role of Extravillous Trophoblast-Derived Exosomes on the Uterine Spiral Arterial Remodeling under Both Normal and Pathological Conditions. *BioMed Res. Int.* **2014**, 693157 (2014).

17. Velicky, P., Knöfler, M. & Pollheimer, J. Function and control of human invasive trophoblast subtypes: Intrinsic vs. maternal control. *Cell Adhes. Migr.* **10**, 154–162 (2015).

18. Cartwright, J. E. *et al.* Trophoblast Invasion of Spiral Arteries: a Novel In Vitro Model. *Placenta* **23**, 232–235 (2002).

19. James, J. L., Whitley, G. S. & Cartwright, J. E. Shear stress and spiral artery remodelling: the effects of low shear stress on trophoblast-induced endothelial cell apoptosis. *Cardiovasc. Res.* **90**, 130–139 (2011).

20. Albrecht, E. D. & Pepe, G. J. Regulation of Uterine Spiral Artery Remodeling: a Review. *Reprod. Sci.* **27**, 1932–1942 (2020).

21. Raghupathy, R. Cytokines as Key Players in the Pathophysiology of Preeclampsia. *Med. Princ. Pract.* **22**, 8–19 (2013).

22. Benyo, D. F., Smarason, A., Redman, C. W., Sims, C. & Conrad, K. P. Expression of inflammatory cytokines in placentas from women with preeclampsia. *J. Clin. Endocrinol. Metab.* **86**, 2505–2512 (2001).

23. Torres-Torres, J. *et al.* A Narrative Review on the Pathophysiology of Preeclampsia. *Int. J. Mol. Sci.* **25**, 7569 (2024).

24. Agarwal, I. & Karumanchi, S. A. Preeclampsia and the Anti-Angiogenic State. *Pregnancy Hypertens.* **1**, 17–21 (2011).

25. Liu, Z., Afink, G. B. & Dijke, P. ten. Soluble fms-like tyrosine kinase 1 and soluble endoglin are elevated circulating anti-angiogenic factors in pre-eclampsia. *Pregnancy Hypertens. Int. J. Womens Cardiovasc. Health* **2**, 358–367 (2012).

26. Margioula-Siarkou, G. *et al.* The role of endoglin and its soluble form in pathogenesis of preeclampsia. *Mol. Cell. Biochem.* **477**, 479–491 (2022).

27. Aouache, R., Biquard, L., Vaiman, D. & Miralles, F. Oxidative Stress in Preeclampsia and Placental Diseases. *Int. J. Mol. Sci.* **19**, 1496 (2018).

28. Mukherjee, I. *et al.* Oxidative stress-induced impairment of trophoblast function causes preeclampsia through the unfolded protein response pathway. *Sci. Rep.* **11**, 18415 (2021).

29. Wang, X. *et al.* VASCULAR AND RENAL MECHANISMS OF PREECLAMPSIA. *Curr. Opin. Physiol.* **33**, 100655 (2023).

30. Powe, C. E., Levine, R. J. & Karumanchi, S. A. Preeclampsia, a Disease of the Maternal Endothelium. *Circulation* **123**, 2856–2869 (2011).

31. Brouwers, L. *et al.* Prevalence of placental bed spiral artery pathology in preeclampsia and fetal growth restriction: A prospective cohort study. *Placenta* **156**, 1–9 (2024).

32. Labarrere, C. A. *et al.* Failure of physiologic transformation of spiral arteries, endothelial and trophoblast cell activation, and acute atherosis in the basal plate of the placenta. *Am. J. Obstet. Gynecol.* **216**, 287.e1-287.e16 (2017).

33. Samantha J. Benton, Katherine Leavey, David Grynspan, Brian J. Cox, & Shannon A. Bainbridge. The clinical heterogeneity of preeclampsia is related to both placental gene expression and placental histopathology. *Am. J. Obstet. Gynecol.* **219**, (2018).

34. Jahan, F., Vasam, G., Green, A. E., Bainbridge, S. A. & Menzies, K. J. Placental Mitochondrial Function and Dysfunction in Preeclampsia. *Int. J. Mol. Sci.* **24**, 4177 (2023).

35. Leavey, K. *et al.* Unsupervised Placental Gene Expression Profiling Identifies Clinically Relevant Subclasses of Human Preeclampsia. *Hypertens. Dallas Tex 1979* **68**, 137–147 (2016).

36. Leavey, K., Bainbridge, S. A. & Cox, B. J. Large Scale Aggregate Microarray Analysis Reveals Three Distinct Molecular Subclasses of Human Preeclampsia. *PLOS ONE* **10**, e0116508 (2015).

37. Leavey, K., Wilson, S. L., Bainbridge, S. A., Robinson, W. P. & Cox, B. J. Epigenetic regulation of placental gene expression in transcriptional subtypes of preeclampsia. *Clin. Epigenetics* **10**, 28 (2018).

38. Harmon, A. C. *et al.* The role of inflammation in the pathology of preeclampsia. *Clin. Sci. Lond. Engl. 1979* **130**, 409–419 (2016).

39. Leavey, K., Grynspan, D. & Cox, B. J. Both 'canonical' and 'immunological' preeclampsia subtypes demonstrate changes in placental immune cell composition. *Placenta* **83**, 53–56 (2019).

40. Than, N. G. *et al.* Early pathways, biomarkers, and four distinct molecular subclasses of preeclampsia: The intersection of clinical, pathological, and high-dimensional biology studies. *Placenta* **125**, 10–19 (2022).

41. Bernier, E. *et al.* Circulating Immune Cells from Early- and Late-onset Pre-eclampsia Displays Distinct Profiles with Differential Impact on Endothelial Activation. *J. Immunol. Author Choice* **213**, 1292–1304 (2024).

42. Arriaga-Pizano, L. *et al.* The Predominant Th1 Cytokine Profile in Maternal Plasma of Preeclamptic Women Is Not Reflected in the Choriodecidual and Fetal Compartments. *J. Soc. Gynecol. Investig.* **12**, 335–342 (2005).

43. Fakhr, Y., Koshti, S., Habibyan, Y. B., Webster, K. & Hemmings, D. G. Tumor Necrosis Factor-α Induces a Preeclamptic-like Phenotype in Placental Villi via Sphingosine Kinase 1 Activation. *Int. J. Mol. Sci.* **23**, 3750 (2022).

44. Romanowska-Próchnicka, K. *et al.* The Role of TNF-α and Anti-TNF-α Agents during Preconception, Pregnancy, and Breastfeeding. *Int. J. Mol. Sci.* **22**, 2922 (2021).

45. Hussain, T. *et al.* The Role of Oxidative Stress and Antioxidant Balance in Pregnancy. *Mediators Inflamm.* **2021**, 9962860 (2021).

46. Liu, Z. *et al.* Role of ROS and Nutritional Antioxidants in Human Diseases. *Front. Physiol.* **9**, (2018).

47. Guo, C., Sun, L., Chen, X. & Zhang, D. Oxidative stress, mitochondrial damage and neurodegenerative diseases. *Neural Regen. Res.* **8**, 2003–2014 (2013).

48. Deluao, J. C. *et al.* OXIDATIVE STRESS AND REPRODUCTIVE FUNCTION: Reactive oxygen species in the mammalian pre-implantation embryo. *Reproduction* **164**, F95–F108 (2022).

49. Grzeszczak, K., Łanocha-Arendarczyk, N., Malinowski, W., Ziętek, P. & Kosik-Bogacka, D. Oxidative Stress in Pregnancy. *Biomolecules* **13**, 1768 (2023).

50. Pashkovskaia, N., Gey, U. & Rödel, G. Mitochondrial ROS direct the differentiation of murine pluripotent P19 cells. *Stem Cell Res.* **30**, 180–191 (2018).

51. Pereira, R. D. *et al.* Angiogenesis in the Placenta: The Role of Reactive Oxygen Species Signaling. *BioMed Res. Int.* **2015**, 814543 (2015).

52. Yang, Y. *et al.* Reactive Oxygen Species are Essential for Placental Angiogenesis During Early Gestation. *Oxid. Med. Cell. Longev.* **2022**, 4290922 (2022).

53. Gupta, S. K., Malhotra, S. S., Malik, A., Verma, S. & Chaudhary, P. Cell Signaling Pathways Involved During Invasion and Syncytialization of Trophoblast Cells. *Am. J. Reprod. Immunol.* **75**, 361–371 (2016).

54. Nadeau, V. & Charron, J. Essential role of the ERK/MAPK pathway in blood-placental barrier formation. *Development* **141**, 2825–2837 (2014).

55. Glutathione: new roles in redox signaling for an old antioxidant - PMC. https://pmc.ncbi.nlm.nih.gov/articles/PMC4144092/#.

56. Chiarello, D. I. *et al.* Oxidative stress: Normal pregnancy versus preeclampsia. *Biochim. Biophys. Acta BBA - Mol. Basis Dis.* **1866**, 165354 (2020).

57. Poston, L. *et al.* Role of oxidative stress and antioxidant supplementation in pregnancy disorders1234. *Am. J. Clin. Nutr.* **94**, S1980–S1985 (2011).

58. Marín, R. *et al.* Oxidative stress and mitochondrial dysfunction in early-onset and late-onset preeclampsia. *Biochim. Biophys. Acta BBA - Mol. Basis Dis.* **1866**, 165961 (2020).

59. Taravati, A. & Tohidi, F. Comprehensive analysis of oxidative stress markers and antioxidants status in preeclampsia. *Taiwan. J. Obstet. Gynecol.* **57**, 779–790 (2018).

60. Holland, O. J. *et al.* Placental mitochondrial adaptations in preeclampsia associated with progression to term delivery. *Cell Death Dis.* **9**, 1150 (2018).

61. Moldogazieva, N. T., Zavadskiy, S. P., Astakhov, D. V. & Terentiev, A. A. Lipid peroxidation: Reactive carbonyl species, protein/DNA adducts, and signaling switches in oxidative stress and cancer. *Biochem. Biophys. Res. Commun.* **687**, 149167 (2023).

62. Sharma, P., Jha, A. B., Dubey, R. S. & Pessarakli, M. Reactive Oxygen Species, Oxidative Damage, and Antioxidative Defense Mechanism in Plants under Stressful Conditions. *J. Bot.* **2012**, 217037 (2012).

63. Iqbal, M. J. *et al.* Interplay of oxidative stress, cellular communication and signaling pathways in cancer. *Cell Commun. Signal.* **22**, 7 (2024).

64. Gonos, E. S. *et al.* Origin and pathophysiology of protein carbonylation, nitration and chlorination in age-related brain diseases and aging. *Aging* **10**, 868–901 (2018).

65. Andrés, C. M. C., de la Lastra, J. M. P., Juan, C. A., Plou, F. J. & Pérez-Lebeña, E. Chemical Insights into Oxidative and Nitrative Modifications of DNA. *Int. J. Mol. Sci.* **24**, 15240 (2023).

66. Obermann, T. *et al.* Genomic 8-oxoguanine modulates gene transcription independent of its repair by DNA glycosylases OGG1 and MUTYH. *Redox Biol.* **79**, 103461 (2025).

67. Wang, J. *et al.* Reassessing the roles of oxidative DNA base lesion 8-oxoGua and repair enzyme OGG1 in tumorigenesis. *J. Biomed. Sci.* **32**, 1 (2025).

68. Nakabeppu, Y. Cellular Levels of 8-Oxoguanine in either DNA or the Nucleotide Pool Play Pivotal Roles in Carcinogenesis and Survival of Cancer Cells. *Int. J. Mol. Sci.* **15**, 12543–12557 (2014).

69. Hahm, J. Y., Park, J., Jang, E.-S. & Chi, S. W. 8-Oxoguanine: from oxidative damage to epigenetic and epitranscriptional modification. *Exp. Mol. Med.* **54**, 1626–1642 (2022).

70. Straszewski-Chavez, S. L., Abrahams, V. M. & Mor, G. The Role of Apoptosis in the Regulation of Trophoblast Survival and Differentiation during Pregnancy. *Endocr. Rev.* **26**, 877–897 (2005).

71. Sharp, A. N., Heazell, A. E. P., Crocker, I. P. & Mor, G. Placental Apoptosis in Health and Disease. *Am. J. Reprod. Immunol. N. Y. N 1989* **64**, 159–169 (2010).

72. Schoots, M. H., Gordijn, S. J., Scherjon, S. A., van Goor, H. & Hillebrands, J.-L. Oxidative stress in placental pathology. *Placenta* **69**, 153–161 (2018).

73. Brooker, I. A., Fisher, J. J., Sutherland, J. M. & Pringle, K. G. Understanding the impact of placental oxidative and nitrative stress in pregnancies complicated by fetal growth restriction. *Placenta* **158**, 318–328 (2024).

74. Voros, C. *et al.* The Role of Placental Mitochondrial Dysfunction in Adverse Perinatal Outcomes: A Systematic Review. *J. Clin. Med.* **14**, 3838 (2025).

75. Fisher, J. J., Bartho, L. A., Perkins, A. V. & Holland, O. J. Placental mitochondria and reactive oxygen species in the physiology and pathophysiology of pregnancy. *Clin. Exp. Pharmacol. Physiol.* **47**, 176–184 (2020).

76. Marschalek, J. *et al.* Maternal serum mitochondrial DNA (mtDNA) levels are elevated in preeclampsia – A matched case-control study. *Pregnancy Hypertens.* **14**, 195–199 (2018).

77. Hu, X.-Q. & Zhang, L. Mitochondrial Dysfunction in the Pathogenesis of Preeclampsia. *Curr. Hypertens. Rep.* **24**, 157–172 (2022).

78. Chen, W., Zhao, H. & Li, Y. Mitochondrial dynamics in health and disease: mechanisms and potential targets. *Signal Transduct. Target. Ther.* **8**, 333 (2023).

79. Correia, Y., Scheel, J., Gupta, S. & Wang, K. Placental mitochondrial function as a driver of angiogenesis and placental dysfunction. *Biol. Chem.* **402**, 887–909 (2021).

80. Bartho, L. A., Fisher, J. J., Cuffe, J. S. M. & Perkins, A. V. Mitochondrial transformations in the aging human placenta. *Am. J. Physiol.-Endocrinol. Metab.* **319**, E981–E994 (2020).

81. Aye, I. L. M. H., Aiken, C. E., Charnock-Jones, D. S. & Smith, G. C. S. Placental energy metabolism in health and disease—significance of development and implications for preeclampsia. *Am. J. Obstet. Gynecol.* **226**, S928–S944 (2022).

82. Voros, C. *et al.* The Role of Placental Mitochondrial Dysfunction in Adverse Perinatal Outcomes: A Systematic Review. *J. Clin. Med.* **14**, 3838 (2025).

83. Wei, L. *et al.* The Role of Placental MFF-Mediated Mitochondrial Fission in Gestational Diabetes Mellitus. *Diabetes Metab. Syndr. Obes.* **18**, 541–554 (2025).

84. Wu, Y. *et al.* Mitochondrial quality control alterations and placenta-related disorders. *Front. Physiol.* **15**, (2024).

85. Ivankovic, D., Chau, K.-Y., Schapira, A. H. V. & Gegg, M. E. Mitochondrial and lysosomal biogenesis are activated following PINK1/parkin-mediated mitophagy. *J. Neurochem.* **136**, 388–402 (2016).

86. Vishnyakova, P. A. *et al.* Mitochondrial role in adaptive response to stress conditions in preeclampsia. *Sci. Rep.* **6**, 32410 (2016).

87. Pandey, D. *et al.* Mitochondrial DNA copy number variation – A potential biomarker for early onset preeclampsia. *Pregnancy Hypertens.* **23**, 1–4 (2021).

88. Taylor, B. D. *et al.* The impact of female fetal sex on preeclampsia and the maternal immune milieu. *Pregnancy Hypertens.* **12**, 53–57 (2018).

89. Muralimanoharan, S., Maloyan, A. & Myatt, L. Evidence of sexual dimorphism in the placental function with severe preeclampsia. *Placenta* **34**, 10.1016/j.placenta.2013.09.015 (2013).

90. Toledano, J. M. *et al.* Pregnancy Disorders: A Potential Role for Mitochondrial Altered Homeostasis. *Antioxidants* **13**, 979 (2024).

91. Jiang, S. *et al.* Effects of maternal diabetes and fetal sex on human placenta mitochondrial biogenesis. *Placenta* **57**, 26–32 (2017).

92. Hebert, J. F. & Myatt, L. Placental mitochondrial dysfunction with metabolic diseases: therapeutic approaches. *Biochim. Biophys. Acta Mol. Basis Dis.* **1867**, 165967 (2021).

93. Steier, J. A., Ulstein, M. & Myking, O. L. Human Chorionic Gonadotropin and Testosterone in Normal and Preeclamptic Pregnancies in Relation to Fetal Sex. *Obstet. Gynecol.* **100**, 552 (2002).

94. Qiu, C., Hevner, K., Enquobahrie, D. A. & Williams, M. A. A case-control study of maternal blood mitochondrial DNA copy number and preeclampsia risk. *Int. J. Mol. Epidemiol. Genet.* **3**, 237–244 (2012).

95. Chin, H.-L., Lai, P. S. & Tay, S. K. H. A clinical approach to diagnosis and management of mitochondrial myopathies. *Neurotherapeutics* **21**, e00304 (2024).

96. Wang, Y. & Walsh, S. W. Placental mitochondria as a source of oxidative stress in pre-eclampsia. *Placenta* **19**, 581–586 (1998).

97. Jauniaux, E. *et al.* Onset of Maternal Arterial Blood Flow and Placental Oxidative Stress: A Possible Factor in Human Early Pregnancy Failure. *Am. J. Pathol.* **157**, 2111–2122 (2000).

98. Morales, J. C. *et al.* Review of Poly (ADP-ribose) Polymerase (PARP) Mechanisms of Action and Rationale for Targeting in Cancer and Other Diseases. *Crit. Rev. Eukaryot. Gene Expr.* **24**, 15–28 (2014).

99. Mao, K. & Zhang, G. The role of PARP1 in neurodegenerative diseases and aging. *FEBS J.* **289**, 2013–2024 (2022).

100. Ke, Y. *et al.* The Role of PARPs in Inflammation—And Metabolic—Related Diseases: Molecular Mechanisms and Beyond. *Cells* **8**, 1047 (2019).

101. Gibson, B. A. & Kraus, W. L. New insights into the molecular and cellular functions of poly(ADP-ribose) and PARPs. *Nat. Rev. Mol. Cell Biol.* **13**, 411–424 (2012).

102. Zhu, H., Tang, Y.-D., Zhan, G., Su, C. & Zheng, C. The Critical Role of PARPs in Regulating Innate Immune Responses. *Front. Immunol.* **12**, (2021).

103. Ortega, R., Bitler, B. G. & Arnoult, N. Multiple functions of PARP1 in the repair of DNA double strand breaks. *DNA Repair* 103873 (2025) doi:10.1016/j.dnarep.2025.103873.

104. Aberle, L. *et al.* PARP1 catalytic variants reveal branching and chain length-specific functions of poly(ADP-ribose) in cellular physiology and stress response. *Nucleic Acids Res.* **48**, 10015–10033 (2020).

105. Ayyappan, V. *et al.* ADPriboDB 2.0: an updated database of ADP-ribosylated proteins. *Nucleic Acids Res.* **49**, D261–D265 (2021).

106. Vivelo, C. A., Wat, R., Agrawal, C., Tee, H. Y. & Leung, A. K. L. ADPriboDB: The database of ADP-ribosylated proteins. *Nucleic Acids Res.* **45**, D204–D209 (2017).

107. Berger, N. A. Poly(ADP-ribose) in the cellular response to DNA damage. *Radiat. Res.* **101**, 4–15 (1985).

108. Spiegel, J. O., Van Houten, B. & Durrant, J. D. PARP1: Structural insights and pharmacological targets for inhibition. *DNA Repair* **103**, 103125 (2021).

109. Chen, Q., Kassab, M. A., Dantzer, F. & Yu, X. PARP2 mediates branched poly ADP-ribosylation in response to DNA damage. *Nat. Commun.* **9**, 3233 (2018).

110. Zhang, H. & Zha, S. The dynamics and regulation of PARP1 and PARP2 in response to DNA damage and during replication. *DNA Repair* **140**, 103690 (2024).

111. Muoio, D. *et al.* PARP2 promotes Break Induced Replication-mediated telomere fragility in response to replication stress. *Nat. Commun.* **15**, 2857 (2024).

112. Kelleher, A. M. *et al.* Deficiency of PARP-1 and PARP-2 in the mouse uterus results in decidualization failure and pregnancy loss. *Proc. Natl. Acad. Sci. U. S. A.* **118**, e2109252118 (2021).

113. Haikarainen, T., Krauss, S. & Lehtiö, L. Tankyrases: Structure, Function and Therapeutic Implications in Cancer. *Curr. Pharm. Des.* **20**, 6472–6488 (2014).

114. Morales, J. C. *et al.* Review of Poly (ADP-ribose) Polymerase (PARP) Mechanisms of Action and Rationale for Targeting in Cancer and Other Diseases. *Crit. Rev. Eukaryot. Gene Expr.* **24**, 15–28 (2014).

115. Bhardwaj, A., Yang, Y., Ueberheide, B. & Smith, S. Whole proteome analysis of human tankyrase knockout cells reveals targets of tankyrase-mediated degradation. *Nat. Commun.* **8**, 2214 (2017).

116. Ge, M. *et al.* DNA damage induced PARP-1 overactivation confers paclitaxel-induced neuropathic pain by regulating mitochondrial oxidative metabolism. *CNS Neurosci. Ther.* **30**, e70012 (2024).

117. Alkylating DNA damage stimulates a regulated form of necrotic cell death. - Google Search. https://www.google.com/search?client=safari&rls=en&q=Alkylating+DNA+damage+stimulates+a+regulated+form+of+necrotic+cell+death.&ie=UTF-8&oe=UTF-8.

118. Ying, W., Garnier, P. & Swanson, R. A. NAD+ repletion prevents PARP-1-induced glycolytic blockade and cell death in cultured mouse astrocytes. *Biochem. Biophys. Res. Commun.* **308**, 809–813 (2003).

119. Zhang, J., Dawson, V. L., Dawson, T. M. & Snyder, S. H. Nitric Oxide Activation of Poly(ADP-Ribose) Synthetase in Neurotoxicity. *Science* **263**, 687–689 (1994).

120. Jahan, F. *et al.* NAD+ depletion is central to placental dysfunction in an inflammatory subclass of preeclampsia. *Life Sci. Alliance* **7**, (2024).

121. Ba, X. & Garg, N. J. Signaling Mechanism of Poly(ADP-Ribose) Polymerase-1 (PARP-1) in Inflammatory Diseases. *Am. J. Pathol.* **178**, 946–955 (2011).

122. Hurtado-Bagès, S., Knobloch, G., Ladurner, A. G. & Buschbeck, M. The taming of PARP1 and its impact on NAD+ metabolism. *Mol. Metab.* **38**, 100950 (2020).

123. Murata, M. M. *et al.* NAD+ consumption by PARP1 in response to DNA damage triggers metabolic shift critical for damaged cell survival. *Mol. Biol. Cell* **30**, 2584–2597 (2019).

124. Walsh, C. S. Two decades beyond BRCA1/2: Homologous recombination, hereditary cancer risk and a target for ovarian cancer therapy. *Gynecol. Oncol.* **137**, 343–350 (2015).

125. Habaka, M. *et al.* PARP Inhibitors in the Neoadjuvant Setting; A Comprehensive Overview of the Rationale for their Use, Past and Ongoing Clinical Trials. *Curr. Oncol. Rep.* **27**, 533–551 (2025).

126. Rose, M., Burgess, J. T., O'Byrne, K., Richard, D. J. & Bolderson, E. PARP Inhibitors: Clinical Relevance, Mechanisms of Action and Tumor Resistance. *Front. Cell Dev. Biol.* **8**, 564601 (2020).

127. Dibitetto, D., Widmer, C. A. & Rottenberg, S. PARPi, BRCA, and gaps: controversies and future research. *Trends Cancer* **10**, 857–869 (2024).

128. Chen, A. PARP inhibitors: its role in treatment of cancer. *Chin. J. Cancer* **30**, 463–471 (2011).

129. Zhou, P., Wang, J., Mishail, D. & Wang, C.-Y. Recent advancements in PARP inhibitors-based targeted cancer therapy. *Precis. Clin. Med.* **3**, 187–201 (2020).

130. Zhu, H. *et al.* A novel TNKS/USP25 inhibitor blocks the Wnt pathway to overcome multi-drug resistance in TNKS-overexpressing colorectal cancer. *Acta Pharm. Sin. B* **14**, 207–222 (2024).

131. Mariotti, L., Pollock, K. & Guettler, S. Regulation of Wnt/β-catenin signalling by tankyrase-dependent poly(ADP-ribosyl)ation and scaffolding. *Br. J. Pharmacol.* **174**, 4611–4636 (2017).

132. Huang, S.-M. A. *et al.* Tankyrase inhibition stabilizes axin and antagonizes Wnt signalling. *Nature* **461**, 614–620 (2009).

133. Tian, X.-H. *et al.* XAV939, a tankyrase 1 inhibitior, promotes cell apoptosis in neuroblastoma cell lines by inhibiting Wnt/β-catenin signaling pathway. *J. Exp. Clin. Cancer Res.* **32**, 100 (2013).

134. Zhang, Y. *et al.* ZEB2 reduction contributes to pre-eclampsia via Wnt/β-Catenin pathway. *Cell Div.* **19**, 34 (2024).

135. Alano, C. C. *et al.* NAD+ Depletion Is Necessary and Sufficient forPoly(ADP-Ribose) Polymerase-1-Mediated Neuronal Death. *J. Neurosci.* **30**, 2967–2978 (2010).

136. Hurtado-Bagès, S., Knobloch, G., Ladurner, A. G. & Buschbeck, M. The taming of PARP1 and its impact on NAD+ metabolism. *Mol. Metab.* **38**, 100950 (2020).

137. Amjad, S. *et al.* Role of NAD+ in regulating cellular and metabolic signaling pathways. *Mol. Metab.* **49**, 101195 (2021).

138. Covarrubias, A. J., Perrone, R., Grozio, A. & Verdin, E. NAD+ metabolism and its roles in cellular processes during ageing. *Nat. Rev. Mol. Cell Biol.* **22**, 119–141 (2021).

139. Berthiaume, J. M., Kurdys, J. G., Muntean, D. M. & Rosca, M. G. Mitochondrial NAD+/NADH Redox State and Diabetic Cardiomyopathy. *Antioxid. Redox Signal.* **30**, 375–398 (2019).

140. Santidrian, A. F. *et al.* Mitochondrial complex I activity and NAD+/NADH balance regulate breast cancer progression. *J. Clin. Invest.* **123**, 1068–1081 (2013).

141. Srivastava, S. Emerging therapeutic roles for NAD+ metabolism in mitochondrial and age-related disorders. *Clin. Transl. Med.* **5**, 25 (2016).

142. Mehmel, M., Jovanović, N. & Spitz, U. Nicotinamide Riboside—The Current State of Research and Therapeutic Uses. *Nutrients* **12**, 1616 (2020).

143. Cantó, C., Sauve, A. A. & Bai, P. Crosstalk between poly(ADP-ribose) polymerase and sirtuin enzymes. *Mol. Aspects Med.* **34**, 1168–1201 (2013).

144. Kupis, W., Pałyga, J., Tomal, E. & Niewiadomska, E. The role of sirtuins in cellular homeostasis. *J. Physiol. Biochem.* **72**, 371–380 (2016).

145. Pham, J., Rajan, K. A. N., Li, P. & Parast, M. M. The role of Sirtuin1–PPARγ axis in placental development and function. *J. Mol. Endocrinol.* **60**, R201–R212 (2018).

146. Arul Nambi Rajan, K. *et al.* Sirtuin1 is required for proper trophoblast differentiation and placental development in mice. *Placenta* **62**, 1–8 (2018).

147. Lappas, M. *et al.* SIRT1 Is a Novel Regulator of Key Pathways of Human Labor1. *Biol. Reprod.* **84**, 167–178 (2011).

148. Wątroba, M., Szewczyk, G. & Szukiewicz, D. The Role of Sirtuin-1 (SIRT1) in the Physiology and Pathophysiology of the Human Placenta. *Int. J. Mol. Sci.* **24**, 16210 (2023).

149. Yin, Y. *et al.* SIRT1 inhibits releases of HMGB1 and HSP70 from human umbilical vein endothelial cells caused by IL-6 and the serum from a preeclampsia patient and protects the cells from death. *Biomed. Pharmacother. Biomedecine Pharmacother.* **88**, 449–458 (2017).

150. Viana-Mattioli, S., Nunes, P., Cavalli, R. & Sandrim, V. Analysis of SIRT1 Expression in Plasma and in an In Vitro Model of Preeclampsia. *Oxid. Med. Cell. Longev.* **2020**, 4561083 (2020).

151. Osborne, B., Bentley, N. L., Montgomery, M. K. & Turner, N. The role of mitochondrial sirtuins in health and disease. *Free Radic. Biol. Med.* **100**, 164–174 (2016).

152. Chao, C.-C. *et al.* SRT1720 as an SIRT1 activator for alleviating paraquat-induced models of Parkinson's disease. *Redox Biol.* **58**, 102534 (2022).

153. Zhang, Y. *et al.* SIRT1 prevents cigarette smoking-induced lung fibroblasts activation by regulating mitochondrial oxidative stress and lipid metabolism. *J. Transl. Med.* **20**, 222 (2022).

154. Giovarelli, M. *et al.* The SIRT1 activator SRT2104 exerts exercise mimetic effects and promotes Duchenne muscular dystrophy recovery. *Cell Death Dis.* **16**, 259 (2025).

155. Bai, P. *et al.* PARP-1 inhibition increases mitochondrial metabolism through SIRT1 activation. *Cell Metab.* **13**, 461–468 (2011).

156. Wan, X., Wen, J., Koo, S.-J., Liang, L. Y. & Garg, N. J. SIRT1-PGC1α-NFκB Pathway of Oxidative and Inflammatory Stress during Trypanosoma cruzi Infection: Benefits of SIRT1-Targeted Therapy in Improving Heart Function in Chagas Disease. *PLOS Pathog.* **12**, e1005954 (2016).

157. Wen, J. J., Yin, Y. W. & Garg, N. J. PARP1 depletion improves mitochondrial and heart function in Chagas disease: Effects on POLG dependent mtDNA maintenance. *PLOS Pathog.* **14**, e1007065 (2018).

158. Wan, X. & Garg, N. J. Sirtuin Control of Mitochondrial Dysfunction, Oxidative Stress, and Inflammation in Chagas Disease Models. *Front. Cell. Infect. Microbiol.* **11**, 693051 (2021).

159. A comparison of rat models that best mimic immune-driven preeclampsia in humans. https://www.frontiersin.org/journals/endocrinology/articles/10.3389/fendo.2023.1219205/full.

160. Suarez-Arnedo, A. *et al.* An image J plugin for the high throughput image analysis of in vitro scratch wound healing assays. *PLoS ONE* **15**, e0232565 (2020).

161. Farrell, R. E. Chapter 6 - Quality Control for RNA Preparations. in *RNA Methodologies (Fifth Edition)* (ed. Farrell, R. E.) 167–185 (Academic Press, 2017). doi:10.1016/B978-0-12-804678-4.00006-3.

162. Jahan, F., Vasam, G., Green, A. E., Bainbridge, S. A. & Menzies, K. J. Placental Mitochondrial Function and Dysfunction in Preeclampsia. *Int. J. Mol. Sci.* **24**, 4177 (2023).

163. Piao, L., Fujioka, K., Nakakido, M. & Hamamoto, R. Regulation of poly(ADP-Ribose) polymerase 1 functions by post-translational modifications. *Front. Biosci.-Landmark* **23**, 13–26 (2018).

164. Xie, N. *et al.* NAD+ metabolism: pathophysiologic mechanisms and therapeutic potential. *Signal Transduct. Target. Ther.* **5**, 227 (2020).

165. Chen, X. *et al.* Role of Reactive Oxygen Species in Tumor Necrosis Factor-alpha Induced Endothelial Dysfunction. *Curr. Hypertens. Rev.* **4**, 245–255 (2008).

166. Jang, D. *et al.* The Role of Tumor Necrosis Factor Alpha (TNF-α) in Autoimmune Disease and Current TNF-α Inhibitors in Therapeutics. *Int. J. Mol. Sci.* **22**, 2719 (2021).

167. Popa, C., Netea, M. G., van Riel, P. L. C. M., van der Meer, J. W. M. & Stalenhoef, A. F. H. The role of TNF-α in chronic inflammatory conditions, intermediary metabolism, and cardiovascular risk. *J. Lipid Res.* **48**, 751–762 (2007).

168. Domercq, M. *et al.* Zn2+-induced ERK activation mediates PARP-1-dependent ischemic-reoxygenation damage to oligodendrocytes. *Glia* **61**, 383–393 (2013).

169. Syed Mortadza, S. A., Mohamad Zahir, N. Z., Wei, C. T. & Jiang, L.-H. The PKC/NOX/ROS and PYK2/MEK/ERK/PARP signalling pathways drive TRPM2 channel activation induced by non-cytolytic oxidative stress in microglial cells. *Redox Rep. Commun. Free Radic. Res.* **30**, 2503131.

170. Pazzaglia, S. & Pioli, C. Multifaceted Role of PARP-1 in DNA Repair and Inflammation: Pathological and Therapeutic Implications in Cancer and Non-Cancer Diseases. *Cells* **9**, 41 (2019).

171. Nakajima, H. *et al.* Critical Role of the Automodification of Poly(ADP-ribose) Polymerase-1 in Nuclear Factor-κB-dependent Gene Expression in Primary Cultured Mouse Glial Cells*. *J. Biol. Chem.* **279**, 42774–42786 (2004).

172. NF-κB and Poly (ADP-ribose) Polymerase 1 Form a Positive Feedback Loop that Regulates DNA Repair in Acute Myeloid Leukemia Cells - PubMed. https://pubmed.ncbi.nlm.nih.gov/30559256/.

173. Zhao, S. *et al.* Compartmentalized regulation of NAD+ by Di (2-ethyl-hexyl) phthalate induces DNA damage in placental trophoblast. *Redox Biol.* **55**, 102414 (2022).

174. Fouquerel, E. *et al.* ARTD1/PARP1 Negatively Regulates Glycolysis by Inhibiting Hexokinase 1 Independent of NAD+ Depletion. *Cell Rep.* **8**, 1819–1831 (2014).

175. Wright, R. H. G. *et al.* CDK2-dependent activation of PARP-1 is required for hormonal gene regulation in breast cancer cells. *Genes Dev.* **26**, 1972–1983 (2012).

176. Yang, B. *et al.* Unveiling anti-oxidative and anti-inflammatory effects of docosahexaenoic acid and its lipid peroxidation product on lipopolysaccharide-stimulated BV-2 microglial cells. *J. Neuroinflammation* **15**, 202 (2018).

177. Ishikado, A. *et al.* 4-Hydroxy hexenal derived from docosahexaenoic acid protects endothelial cells via Nrf2 activation. *PloS One* **8**, e69415 (2013).

178. Kang, D. H., Lee, J. H. S. & Kang, S. W. Survival of APC-mutant colorectal cancer cells requires interaction between tankyrase and a thiol peroxidase, peroxiredoxin II. *BMB Rep.* **50**, 391–392 (2017).

179. Sharma, S. *et al.* Electrophilic Aldehyde 4-Hydroxy-2-Nonenal Mediated Signaling and Mitochondrial Dysfunction. *Biomolecules* **12**, 1555 (2022).

180. Patergnani, S., Bouhamida, E., Leo, S., Pinton, P. & Rimessi, A. Mitochondrial Oxidative Stress and "Mito-Inflammation": Actors in the Diseases. *Biomedicines* **9**, 216 (2021).

181. Rymer-Haskel, N. *et al.* Characteristics and severity of preeclampsia in young and elderly gravidas with hypertensive disease. *Eur. J. Obstet. Gynecol. Reprod. Biol.* **228**, 120–125 (2018).

182. Liu, Y. *et al.* The metabolic role of LncZBTB39-1:2 in the trophoblast mobility of preeclampsia. *Genes Dis.* **5**, 235–244 (2018).

183. Fajardy, I. *et al.* Time course analysis of RNA stability in human placenta. *BMC Mol. Biol.* **10**, 21 (2009).